RESEARCH ARTICLE

Enhancing lipid production in plant cells through automated high-throughput genome editing and phenotyping

Jia Dong[1,2,3,11], Seth W. Croslow[2,4,5,11], Stephan T. Lane[2,3], Daniel C. Castro[5,6], Jantana Blanford[7], Shuaizhen Zhou[2,3], Kiyoul Park[8,9], Steven Burgess[10], Mike Root[3], Edgar Cahoon[8,9], John Shanklin[7], Jonathan V. Sweedler[2,3,4,5,6*†], Huimin Zhao[2,3,4*†], Matthew E. Hudson[1,2,3*†]

[1]Department of Crop Sciences, University of Illinois at Urbana-Champaign, Urbana, IL, USA.

[2]Department of Energy Center for Advanced Bioenergy and Bioproducts Innovation, University of Illinois at Urbana-Champaign, Urbana, IL, USA.

[3]Carl R. Woese Institute for Genomic Biology, University of Illinois at Urbana-Champaign, Urbana, IL, USA.

[4]Department of Chemistry, University of Illinois Urbana-Champaign, Urbana, IL, USA.

[5]Beckman Institute for Advanced Science and Technology, University of Illinois at Urbana-Champaign, Urbana, IL, USA.

[6]Department of Molecular and Integrative Physiology, University of Illinois at Urbana-Champaign, Urbana, IL, USA.

[7]Biology Department, Brookhaven National Laboratory, Upton, NY, USA.

[8]Center for Plant Science Innovation, University of Nebraska–Lincoln, Lincoln, NE, USA.

[9]Department of Biochemistry, University of Nebraska–Lincoln, Lincoln, NE, USA.

[10]School of Integrative Biology, University of Illinois at Urbana-Champaign, Urbana, IL, USA.

[11]These authors contributed equally: Jia Dong, Seth W. Croslow.

Short title: Lipid enhancement via an automated platform

[*]Corresponding authors:
[†]Matthew Hudson: mhudson@illinois.edu; Huimin Zhao: zhao5@illinois.edu; Jonathan Sweedler: jsweedle@illinois.edu.

The author responsible for distribution of materials integral to the findings presented in this article in accordance with the policy described in the Instructions for Authors

(https://academic.oup.com/plcell/pages/General-Instructions) is Matthew Hudson (mhudson@illinois.edu).

Abstract

Plant bioengineering is a time-consuming and labor-intensive process with no guarantee of achieving desired traits. Here, we present a fast, automated, scalable, high-throughput pipeline for plant bioengineering (FAST-PB) in maize (*Zea mays*) and *Nicotiana benthamiana*. FAST-PB enables genome editing and product characterization by integrating automated biofoundry engineering of callus and protoplast cells with single-cell matrix-assisted laser desorption/ionization mass spectrometry (MALDI-MS). We first demonstrated that FAST-PB could streamline Golden Gate cloning, with the capacity to construct 96 vectors in parallel. Using FAST-PB in protoplasts, we found that PEG2050 increased transfection efficiency by over 45%. For proof-of-concept, we established a reporter-gene-free method for CRISPR editing and phenotyping via mutation of *high chlorophyl fluorescence 136* (*HCF136*). We show that diverse lipids were enhanced up to sixfold using CRISPR activation of lipid controlling genes. In callus cells, an automated transformation platform was employed to regenerate plants with enhanced lipid traits through introducing multi-gene cassettes. Lastly, FAST-PB enabled high-throughput single-cell lipid profiling by integrating MALDI-MS with the biofoundry, protoplast, and callus cells, differentiating engineered and unengineered cells using single-cell lipidomics. These innovations massively increase the throughput of synthetic biology, genome editing, and metabolic engineering and change what is possible using single-cell metabolomics in plants.

Introduction

Plant genetic engineering is needed more than ever to maintain global food security while battling ever-changing environmental conditions. Currently, engineering plants with desired traits is a complex and intricate process demanding significant time and labor (Mumm, 2013). This process involves several key steps, including gene construct design, plant transformation or transfection, genome editing, and analysis and screening to identify the desired traits (Karlson et al., 2021; Yin et al., 2017). As a result, the development of engineered plants is typically a low-throughput and labor-intensive process, and represents one of the major limitations in plant biotechnology (Huang et al., 2022). Our research focuses on engineering plants for enhanced vegetative lipid production, a promising avenue to improve global plant oil production without the need for increased fertilizer or land area use (Napier et al., 2014; Maitra et al., 2022). Achieving stable lipid production in biomass tissues requires the engineering and expression of multiple genes, and prototyping of these multi-gene constructs is a rate-limiting step in developing next-generation crops (Vanhercke et al., 2019, 2014; Volk et al., 2023).

To overcome this limitation, we sought to integrate an automated biofoundry with single-cell metabolomics to expedite the engineering of plant genomes and characterization of cellular effects, which has never been done before. Biofoundries are specialized workstations that integrate robotics, high-throughput instrumentation, computer-aided design, and informatics to speed up iterative biological Design-Build-Test-Learn cycles in a scalable manner (Hillson et al., 2019; Zhang et al., 2021; Chao et al., 2017). These workstations are highly reproducible, and optimize resource utilization by reducing human time and labor costs, increasing experimental throughput, and enabling researchers to devote more time towards experimental design as well as analysis and interpretation of results (Hillson et al., 2019). The Illinois Biological Foundry for Advanced Biomanufacturing (iBioFAB) has demonstrated success in automating synthetic biology processes such as plasmid assembly (Enghiad et al., 2022), yeast genome editing (Si et al., 2017), and antimicrobial discovery (Si et al., 2015). This success paves the way for the development of high-throughput plant genome editing

technologies. Beyond the iBioFAB, it is important to note that biofoundry development has been strongly emphasized worldwide, including the United States, South Korea, China, and others. The U.S. federal government has prioritized the acceleration of Design-Build-Test-Learn capabilities through initiatives such as Executive Order 14081 and subsequent funding opportunities from the National Science Foundation (NSF 24-556 and NSF 23-585). Despite these advances, most biofoundry initiatives have focused on microbial, mammalian, and DNA-based systems, and progress in automating plant biotechnology has been limited (Rigoulot et al., 2023).

Beyond developing engineered plants, a rapid and scalable method for characterizing genome editing is essential for development of a high-throughput platform for plant improvement. Single-cell metabolomics is compatible with high-throughput techniques, allowing the metabolic profiles of individual cells to be determined. Single-cell approaches allow the phenotypic heterogeneity among cells to be investigated (Pandian et al., 2023). They also provide an immediate and dynamic snapshot of an individual cell's functionality (Seydel, 2021). Historically, metabolic data has been collected from cell populations, where average values lead to misleading interpretations about the state of each cell (Ali et al., 2019). Recent studies have shown that measurements of the average metabolome of a cell population conceals important information about the heterogeneity of individual cells, since cells are highly dynamic and constantly interact with each other and their environment (Guo et al., 2021; Lawson et al., 2015). Even two genetically identical cells often display different chemical metabolomes (Seydel, 2021). Therefore, various bioanalytical tools have been developed for measuring single cell metabolomics, one example being matrix-assisted laser desorption/ionization mass spectrometry (MALDI-MS) (Seydel, 2021; Bourceau et al., 2023; Neumann et al., 2019). These methods have recently been applied to lipidome profiling of single cells in the mouse brain (Zhang et al., 2023).

In this work, we have established a fast, automated, scalable, high-throughput pipeline for plant bioengineering (FAST-PB) (Figure 1). This pipeline seamlessly integrates the iBioFAB (Supplementary Figure S1) biofoundry for automated synthetic biology with matrix-assisted laser desorption/ionization Fourier transform ion cyclotron resonance mass spectrometry (MALDI FT-ICR MS) for high-throughput single-cell lipid

identification. FAST-PB is compatible not only with protoplast cells that can be quickly isolated, transfected, and analyzed, but also callus cell cultures that can be maintained indefinitely for long-term studies and regenerated into a mature plant. As a proof of concept, we applied this pipeline to assemble plasmid DNA constructs for plant transformation, engineer two cell factories (protoplast and callus) with a multi-gene stack giving a 2-6-fold improvement in lipid accumulation, and perform lipidomic analysis at the single-cell level in a high-throughput manner. The FAST-PB pipeline integrates three automated workflows, enabling further scientific findings: for the automated protoplast workflow, we first show that FAST-PB can be used for optimization of transfection efficiency in protoplasts, which can reach up to over 45%. Next, to quickly detect genome editing during the validation of our workflow, we developed a reporter gene-free system. Our system determines genome editing efficiency via the knockout of a photosynthetic gene, *high chlorophyll fluorescence 136* (*HCF136*), leading to changes in chlorophyll fluorescence intensity. We then applied this platform to study genes involving lipid pathways, and initially found that the lipids in protoplasts are stable over time, making them a useful platform for lipid engineering. Using this approach, we validated the function of two genes for lipid production, *Diacylglycerol O-acyltransferase 1 (DGAT1)* and *WRINKLED1* (*WRI1*) from *Nicotiana benthamiana* and maize. These two endogenous genes significantly increase the production of a variety of lipids by 2-6 fold when overexpressed using the CRISPR activation system. We have also successfully established an automated callus transformation to facilitate plant regeneration with enhanced lipids traits. Finally, for the combination of callus and protoplast workflow, our high-throughput single-cell lipid profiling differentiates between individual transformed and untransformed cells based on their lipid profile, providing valuable information about how genetic engineering impacts lipid metabolism at the cellular level. Overall, our pipeline has not only greatly accelerated plant transformation, CRISPR genome editing, single cell metabolomics, and plant regeneration, but also enhanced our capacity for scientific findings.

Results

Design of the FAST-PB pipeline

The iBioFAB is an integrated robotic platform that facilitates the development of fully automated workflows for scalable and high-throughput synthetic biology applications. User-defined workflows are encoded into *Momentum* software, which coordinates communication between instruments, control of the robotic arm, and monitors location of the inventory of plates, samples, and consumables. FAST-PB is a *Momentum*-based biotechnology pipeline containing three main modules: (1) Design: CRISPR-P and Benchling online tools are used to design gRNAs and build digital CRISPR vectors containing Cas9 and gRNA sequences. A Golden Gate cloning workflow encoded into the iBioFAB utilizes a Beckman Coulter Echo acoustic liquid handler for preparation of PCR and DNA assembly reactions, an integrated TRobot2 thermocycler for reaction incubations, and a Tecan Fluent pipetting liquid handler for *Escherichia coli* transformations and plasmid extraction (Figure 1A, Supplementary Figures S1 and S2A, Supplementary Table S1). (2) Build: plasmids are transformed into *N. benthamiana* callus suspension cells (Figure 1B, Supplementary Figure S2B) or transfected into protoplast cells derived from maize or *N. benthamiana* leaves (Figure 1C, Supplementary Figures S2C-D). (3) Test: to complete the end-to-end automated trait optimization pipeline, two mass spectrometry methods are integrated for lipid profiling. For single-cell lipid measurements using MALDI-FT-ICR-MS, callus-derived protoplasts are deposited onto indium tin oxide (ITO) coated microscopy slides. The locations of the single cells on the ITO-slide are then determined and probed using the MALDI laser for high-throughput lipid quantification. In addition, genome engineered plant cells can be analyzed via liquid chromatography tandem mass spectrometry (LC-MS/MS) (Figure 1D).

Overall, distinct plant cell systems exhibit unique advantages and disadvantages, with the selection of the optimal cell system often depending upon the specific application at hand. Protoplasts can be rapidly generated and easily chemically transfected but are generally short-lived, rendering them unsuitable for applications requiring complete plant tissues. On the other hand, callus systems are comprised of a mass of

undifferentiated cells which can be maintained for longer periods and regenerated into entire plants (or converted into protoplasts). To develop a versatile platform applicable for the widest variety of plant engineering applications, we designed the FAST-PB platform (Figure 1) for compatibility with both callus tissue (Figure 1A, B, D) and protoplast cells (Figure 1A, C, D) as well as developing a custom technique that synergistically harnesses the benefits of both, by converting callus to protoplasts (Figure 1A-D). Therefore, the FAST-PB platform contains three distinct automated workflows: automated callus transformation (Figure 1A, B, D), automated protoplast isolation and transfection (Figure 1A, C, D), and a combination of callus and protoplast workflow (Figure 1A-D) for single-cell metabolomics.

Automated protoplast isolation and transfection for scalable and rapid genome editing and lipid phenotyping

Genetic engineering of plant cells is challenging because plant cell walls restrict the delivery of exogenous biomolecules (Demirer et al., 2019), and transformation and phenotypic screening is labor intensive (Squire et al., 2023; Lenaghan and Neal Stewart, 2019). Protoplasts offer one potential solution due to their ease of production and transfection. Therefore, we initially established an automated workflow for high-throughput protoplast isolation, transfection, and gene mutant screening.

The first step involved automating protoplast isolation from leaves of both maize and *N. benthamiana*. We translated the manual protocol for protoplast isolation (Supplementary Method 2) into an automated procedure (Supplementary Figure S2C). Briefly, leaf sections were excised and transferred into 24-well v-bottom plates for processing. Samples were then digested, filtered, washed, and resuspended on the Tecan Fluent with required centrifugation steps performed by the F5 robotic arm and integrated centrifuge. Using this workflow, high quality protoplast cells were isolated from both etiolated maize and *N. benthamiana* leaves at a concentration of about 10^6 cells / mL (Figure 2A-B).

Next, we developed an automated workflow for protoplast transfection by encoding an established manual protocol (Supplementary Method 2) into *Momentum* (Supplementary Figure S2D). In general, plasmids, polyethylene glycol (PEG) transfection solution, MMG solution, and protoplast cells were mixed using the Tecan

Fluent, followed by incubation. Subsequently, centrifugation was performed with the assistance of the F5 robotic arm and centrifuge. The washing and resuspension steps were then carried out using Tecan Fluent. We first applied this transfection workflow to optimize transfection efficiency by testing PEG with three different molecular weights: 2050, 3350, and 4000 g/mol. This choice is based on previous studies demonstrating that the molecular weight of PEG influences gene delivery efficiency (Zhang et al., 2008). Our experiments showed that PEG 2050 resulted in the highest fraction of GFP-positive cells (Supplementary Figures S3A-B) with the overall highest number of intact cells in both plants (Figure 2C and Supplementary Figures S3A-B), even though PEG 4000 is the most commonly used molecular weight for protoplast transfection in both *N. benthamiana* and maize. Next, we employed PEG 2050 to transfect cells to assess the viability of cells over time. We calculated the transfection stability over a period of four days by dividing the number of GFP-positive cells by the total number of intact cells. The largest proportion of cells expressing GFP was observed during the first two days in *N. benthamiana* and the first three days in maize, reaching up to 41% and 57% for maize and *N. benthamiana*, respectively (Figure 2D), but declined in the following days (Supplementary Figures S3C-D).

To demonstrate genome editing using automated protoplast isolation and transfection, we developed a reporter-gene-free cellular assay for loss of gene function. This endogenous genome-editing assay is based on a single gene, *HCF136*, that increases chlorophyll fluorescence when its function is lost (Meurer et al., 1998). We used this assay to determine the effectiveness of the automated protoplast-editing procedures using a simple plate reader assay for differential chlorophyll fluorescence. First, we isolated cells from both maize and *N. benthamiana* leaves, then the two cell types were individually transfected with CRISPR knockout plasmids: P-A0502 (negative control) and P-A0502-HCF136 for *N. benthamiana,* and A1510 (negative control) and A1510-HCF136 for maize (Supplementary Table S1). Each plasmid transfection had 10 replicates, resulting in a total of 40 samples in a 96-well plate. Our results showed that we successfully induced mutations in *HCF136* in protoplast cells from both maize and *N. benthamiana* (Figure 2F), resulting in a significant enhancement in chlorophyll fluorescence intensity, as illustrated in Figure 2E. Thus, automation of protoplast

generation, transfection, and phenotyping can be achieved with FAST-PB. Subsequently, we applied this automated workflow to the study of lipid metabolism and engineering. Lipids in plants serve multiple functions, including energy storage, structural support, protection, and signaling (Okazaki and Saito 2014; Xie et al. 2021). To effectively explore lipid metabolism using protoplasts, it is essential that lipids remain relatively stable throughout the experimental period. Thus, we applied our automated protoplast isolation workflow to measure the lipid content in protoplasts over a four-day period. Apart from a substantial increase in triacylglyceride (TAG) content in *N. benthamiana* over three days, most lipids remained stable for four days in protoplasts of both species (Figure 2G). These results indicate that protoplasts are a suitable and scalable platform for lipid investigations.

We then employed our workflow to investigate several lipid-related genes in both maize and *N. benthamiana*. Previous studies have shown that editing genes involved in fatty acid synthesis ('Push'), TAG assembly ('Pull'), and lipid turnover ('Protect') can significantly affect the accumulation of lipids in plants (Vanhercke et al., 2019, 2014). Specifically, the three genes *WRI1*, *DGAT1*, and *Oleosin* represent push, pull, and protect steps, respectively (Zhai et al., 2017a; Vanhercke et al., 2014). Thus, we applied this workflow to the orthologs of these genes in *N. benthamiana* and maize using CRISPR activation and / or strong promoter systems. *N. benthamiana* protoplast cells were transfected with CRISPR activation vectors: P-A3701 as a control, P-A3701-DGAT1 (Overexpression of *DGAT1*), P-A3701-WRI1 (Overexpression of *WRI1*). Maize protoplast cells were transfected using two different strategies: CRISPR activation and strong promoter. The CRISPR activation group included a control (A4110) and variants containing overexpression of *DGAT1* (A4110-DGAT1), and *WRI1* (A4110-WRI1). The strong promoter controls consisted of a control vector without lipid gene overexpression constructs (pPTN1586C) and the vector pPTN1586, used to overexpress the genes *DGAT1*, *WRI1*, *Oleosin*, *thioesterase (Thio14)*, and *lysophosphatidic acid acyltransferase (LPATB)*. We initially used pPTN1586 as a positive control to validate our automated workflow for lipid studies in maize protoplasts. Preliminary manual experiments showed that transfection with pPTN1586 significantly increased lipid production in maize protoplasts, demonstrating the maize protoplast system is suitable

for lipid studies. Consequently, this vector pPTN1586 was included as a positive control in the automated maize protoplast workflow.

In *N. benthamiana*, overexpression of *WRI1* or *DGAT1* via CRISPR activation increased accumulation of various lipid classes (Figure 2H). In maize, overexpression of either *WRI1,* or *DGAT1* through CRISPR activation also resulted in increased accumulation of many types of lipids (Figure 2H). The same trend was found in the control group after overexpression of five lipid-related genes using strong promoters, but with higher lipid accumulation (Figure 2H). In addition, we confirmed *DGAT1* was overexpressed in response to CRISPR activation in maize cells, using RT-qPCR (Supplementary Figure S4D). Thus, we developed an end-to-end automated pipeline for implementing gene editing and transformation and characterizing lipid profiles using protoplasts in both a monocot and dicot system.

Automated callus cell culture transformation platform enhances lipids production and facilitates plant regeneration

In parallel, we developed an automated callus transformation workflow and integrated it into our FAST-PB pipeline (Supplementary Figure S2B). Unlike protoplasts, plant callus tissue is comprised of an unorganized mass of cells, which can be readily transformed and cultured for long periods (Ikeuchi et al., 2013). These properties make callus tissue a valuable tool for studying plant cell metabolomes, especially lipid metabolism (TSAI et al., 1982; Norouzi et al., 2022). Nonetheless, there is a lack of research on using biofoundries for automating management and transformation of callus cell cultures. Therefore, an automated callus-transformation workflow was developed on the iBioFAB (Supplementary Figure S2B) and utilized to knockout genes via CRISPR genome editing and overexpress target genes driven either by the strong CaMV 35 strong promoter or the CRISPR activation system (Supplementary Figure S4A-C).

As a first proof of concept of our automated callus platform, the *HCF136* gene was again knocked out and confirmed via sequence analysis (Supplementary Figure S4A and S4F). We detected deletion events after CRISPR knockout of the *HCF136* gene. Additionally, we observed the mutated calli appeared yellowish and unhealthy on the MS-selected media compared to the control (Supplementary Figure S4A).

Following this, we applied this automated workflow to assess three distinct lipid genes in the callus system. Callus cultures transformed with an *Oleosin/WRI1/DGAT1* (OWD) overexpression cassette (pMDC43-OWD) driven by the strong, constitutive 35S promoter, or an empty vector control (pMDC43), were confirmed by observation of GFP fluorescence, then stably maintained on selective agar plates (Supplementary Figure S4C, Figure 3J). The lipids and fatty acids in these genetically-engineered calli were then analyzed by LC-MS/MS and GC-MS. Compared to control cells, overexpression of OWD led to increased accumulation of many lipids and fatty acids (Figures 3A, 3D, 3G), indicating the induction of lipid synthesis resulted in cellular lipid accumulation.

In addition to simultaneous overexpression of OWD, we individually overexpressed *DGAT1* (C-A3701-DGAT1), *WRI1* (C-A3701-WRI1) and control (C-A3701) using CRISPR activation (Supplementary Figure S4B) and confirmed that both genes were overexpressed by RT-qPCR (Supplementary Figure S4E). In contrast to simultaneously overexpressing three genes in OWD, individual overexpression of either *WRI1* (Figure 3B) or *DGAT1* (Figure 3C) decreased accumulation of some lipids, although a far larger number either increased or remained unchanged. Overexpression of *WRI1* increased accumulation of a variety of lipids and fatty acids (Figure 3E and 3H) and overexpression of *DGAT1* induced a similar overall profile (Figure 3F and 3I), suggesting that the genetic modification achieved through CRISPR activation successfully induced alteration in lipid composition.

Whole plant regeneration and lipidomic analysis

After confirming an increase of lipid content in these genetically engineered calli, we initiated the process of plant regeneration by transferring them to MS induction media, which resulted in the development of mature plants (Figure 3J). This demonstrates that the FAST-PB automated callus workflow not only enables the designing, building, and testing of engineered plant cells using robotics, but also facilitates the regeneration of whole plants. We then generated three separate transgenic events and regenerated whole *N. benthamiana* plants with overexpression of either *WRI1* or *OWD*, and then profiled leaf tissue from one-month-old seedlings with liquid chromatography-tandem mass spectrometry (LC-MS/MS) lipid assays (Figure 3K and 3L). These results are consistent with those observed in the initial protoplast and callus analysis,

demonstrating that overexpression of *WRI1* alone leads to a significant and consistent increase in TAG and some phospholipid species by approximately 2- to 6-fold. However, overexpression of OWD (*Oleosin, DGAT, and WRI1*) creates an effective push-pull-protect strategy where the levels of most phospholipids return to wild-type levels, and DAG levels are only mildly elevated, whereas TAG levels are increased by more than 15 fold in all of the transgenic events. In addition, to assess the consistency of lipid production during plant growth, we measured lipid production in three-month-old genetically engineered *N. benthamiana* using BODIPY (494/503) lipid staining, thin-layer chromatography (TLC), and LC-MS/MS technology. We found that lipid production was consistently higher in the overexpression group (pMDC43-OWD or A3701-WRI1) than in the control group (pMDC43 or A3701) (Supplementary Figure S5). In addition, we performed lipid profiling on seeds from six independent transgenic events. The results showed that while many types of lipids increased, the changes were not significant (Supplementary Figure S5E).

Taken together, these results demonstrate a scalable pipeline that combines automation, quantitative lipid analysis, transformation, and plant regeneration, with an immediate application in improving plant lipid production.

High-throughput single-cell lipid metabolism analysis achieved via automation integrated with MALDI-MS

Having developed a scalable and automated platform for genetic transformation of both callus and protoplast systems, lipid profiling through LC-MS/MS became the rate-limiting step in our analysis. Compared to other steps in our automated workflow, LC-MS/MS is low throughput, costly, and incompletely compatible with our iBioFAB platform due to the need for lipid extraction, which requires organic solvents and some manual handling. To address these shortfalls and develop a complete end-to-end plant synthetic biology pipeline, we sought to harness the benefits of both protoplast and callus systems through a hybrid approach focused on single cell lipidomic analysis. We started by transforming callus cells using the iBioFAB system to generate stable, genetically-engineered cultures, then performed automated protoplast isolation. We then developed a single-cell MALDI FT-ICR MS lipid analysis pipeline for isolated callus-derived protoplasts (Figure 4A-B).

We started by performing automated protoplast isolation from wildtype callus and then developed a single-cell MALDI-FT-ICR-MS lipidomic analysis pipeline for the isolated protoplasts (Figure 4A-B). Briefly, protoplasts are imaged in the W5 lipid media to check the quality of the cell before MALDI-MS (Figure 4A). Then cells are stained with a nuclear dye, deposited onto an indium tin oxide-coated microscopy slide, imaged under brightfield and fluorescence microscopy, then analyzed individually (Figure 4B). This technique enables automatic, quantitative and cost-effective single-cell lipid measurements with a high analytical throughput. As the first step, we conducted traditional LC-MS/MS lipid profile measurements on bulk isolated protoplasts derived from wild type calli, to ensure the consistency of the datasets obtained from the LC-MS/MS and MALDI-MS. Of the detected lipid types from MALDI-MS, 33% were matched to the LC-MS/MS lipid datasets. Using this workflow, MALDI-MS spectral analysis revealed a variety of lipid types (Figure 4C). All these results indicate that MALDI-MS has the capability to detect a wide range of lipids in individual cells.
We next used this automated callus transformation and protoplast generation workflow to transform plasmids (pMDC43-OWD, pMDC43 as a control; C-A3701-DGAT1, C-A3701-WRI1, C-A3701 as a control) into *N. benthamiana* callus and isolate protoplasts from the genetically engineered calli.

To assess the consistency of lipid profiles between genetically engineered calli and protoplast cells derived from these calli, we directly compared these platforms using bulk LC-MS/MS analysis of pooled protoplasts and callus tissue. Consistent with the results obtained by extracting lipids from genetically engineered transgenic calli for LC-MS/MS, the callus-derived protoplasts exhibited increased lipid accumulation after overexpression of either *WRI1* or *DGAT1* or simultaneous overexpression of the three-gene *OWD* stack (Figure 4D and Supplementary Figure S6), demonstrating that lipid profiles of callus-derived protoplasts represent the original callus.

High-throughput single-cell lipid metabolite profiling was then performed on the callus-derived protoplasts using MALDI-MS. We observed a significant increase in the accumulation of various lipid classes in the MALDI-MS data, particularly TAGs, in response to *OWD* expression (Figure 4E). Single-cell MALDI data was mass matched to the LC-MS/MS datasets for putative lipid assignment (Supplementary Table S2).

MALDI-MS spectral analysis revealed higher levels of several lipid classes after overexpression of 43-OWD when compared against the negative control (Figure 4F-G). These findings indicate that MALDI-MS analysis of protoplasts is a promising method for single-cell lipid measurements in plants.

To ensure the accuracy and reliability of the MALDI-MS method for lipid measurement, we compared single-cell MALDI-MS to the reference method, LC-MS/MS on bulk cells. We found a high degree of consistency between the two datasets, both in terms of lipid classes and species-level trends, such as TAGs (Figure 4H-I). This finding indicates that single protoplast MALDI-FT-ICR-MS facilitates accurate and efficient high-throughput lipid measurement on single plant cells, positioning it as a valuable alternative to the LC-MS/MS approach. Similar results on the comparability and concordance between LC-MS and MALDI-MS have also been recently reported in human cells (Martín-Saiz et al., 2023). Moreover, our single cell measurements and data processing have the capacity to differentiate transformed and untransformed cell types within the 43-OWD group, demonstrating that based on single-cell heterogeneity, we can estimate which protoplasts have been genetically engineered (Supplementary Figure S6E).

Taken together, by coupling callus transformation with protoplast isolation and MALDI-FT-ICR-MS analysis, FAST-PB embodies a high-throughput, automation-friendly, end-to-end pipeline for plant genetic engineering and characterization at the single cell level. This can be used for investigating the effects of specific genetic perturbations on lipid metabolism, and potentially other metabolic pathways.

Discussion

Traditional plant genetic engineering involves labor-intensive, low-throughput processes encompassing gene construction, transfection or transformation, genome editing, mutant identification, gene function analysis, and plant regeneration (Karlson et al., 2021; Yin et al., 2017; Mumm, 2013). To automate these steps and achieve high throughput, we successfully established the FAST-PB pipeline comprising automated gene constructions, protoplast cell isolation and transfection, callus transformation, genomic DNA extraction, and lipid profiling. Protoplasts provide a rapid way to validate

the effectiveness of CRISPR knockout or CRISPR activation on gene expression and serve as a great way to screen large numbers of genes for ones that may affect cellular biochemistry. Callus can be readily converted to protoplasts or regenerated into stable plant lines. Stable transgenic plants, while the ultimate goal of these procedures, are the slowest and most space-dependent of the systems in which to test genes; FAST-PB allows us to test many genes in protoplasts and callus and only to move the most promising ones into stable plants. Our results demonstrate that, compared to the manual protocols, each automated step from the FAST-PB pipeline significantly reduces time and labor (Table S3).

While biofoundries excel in precision, scalability, and cost-efficiency for genome editing and metabolic engineering (Si et al., 2017), they have yet to be applied to plant synthetic biology. Here we fill this gap with our broadly applicable and scalable plant genetic engineering pipeline. Our automated protoplast engineering workflow enables rapid isolation and transfection of up to 96 individual samples in a short amount of time. Another potential benefit of this workflow is the ability to simultaneously optimize multiple parameters (e.g. PEG types, mannitol concentrations, and incubation times) for transfection efficiency. As an example, we were able to quickly optimize transfection efficiency using three PEG batches with different average molecular weights (2050, 3350, and 4000) on the iBioFAB platform, finding that the PEG 2050 consistently enhanced transfection efficiency while preserving the integrity of the protoplast cultures (Figure 2C). Furthermore, we envision applications of our automated protoplast engineering workflow for high-throughput assessments of in vivo gene editing efficiency of specific guide RNAs, subcellular localization experiments via fused fluorescent proteins, or confirmation of protein-protein interactions through bimolecular fluorescence complementation assays. Our automated callus transformation workflow enables simultaneous processing of up to twelve six-well plates at a time for a total throughput of 96 samples and facilitating plant regeneration (Figure 3J), opening the door to high-throughput screening of genes related to whole-plant traits such as plant pathology, biofuel production, and crop yield improvement.

Single-cell technology has gained significant attention in recent years (Roy et al., 2018). Plant tissues encompass a multitude of distinct cell types, each assuming specialized

roles, exhibiting diverse molecular behaviors, and generating unique metabolites in response to biotic and abiotic stresses (Cole et al., 2021). Profiling whole plant tissues using traditional bulk methods can obscure and dilute signals associated with specific single cells. However, plant cell walls and tissue structures tend to complicate single cell analysis. Therefore, we automated the isolation of protoplast cells using the iBioFAB platform, followed by measurement of lipid profiles in each single cell using MALDI/MS technology as a high-throughput single-cell assay, and validation of the results by comparison to lower-throughput LC-MS/MS assays on bulk cells. We were able to measure a wide variety of lipid classes in single cells, including storage lipids (TAG and DAG) and phospholipids (PC, PE, LPC, and LPE) showing comparable results to LC-MS/MS (Figure 4). The greatest advantage of MALDI-MS is that it achieves lipid profiling in just 1-2 seconds per cell, while LC-MS/MS takes approximately 20 minutes per sample (Table S3). In terms of cost, MALDI-MS proves to be more economical, with a current (2025) estimated cost of ~ $0.9 per sample compared to ~ $6 per sample for LC-MS/MS (Table S3). Therefore, the addition of MALDI-MS increases the cost-effectiveness and throughput of FAST-PB.

Single-cell studies with FAST-PB have a variety of potential applications. Previous studies have identified specific cell types related to processes such as oil production (Taylor et al., 2021), plant pathogen responses, and environmental stress (Cole et al., 2021). Our platform enables quickly transfecting cells for high-throughput gene analysis and enables dissection of gene function at the single cell level. Moreover, our workflows can accelerate genomic and metabolic engineering processes within cell factories, facilitating plant transformation and regeneration. Lastly, within each cell, various types of organelles / vesicles play a role in disease or stress tolerance (Urzì et al., 2021; Cui et al., 2020). Recent reports demonstrate the ability of MALDI-MS to probe these subcellular structures (Castro et al., 2021; Eberwine et al., 2023; Castro et al., 2023), although not all these methods have yet been applied to characterizing plant vesicles, which may be the site of at least some of the increased cellular phospholipid content of some of the engineered cells described in this report. The ability to examine the contents of these subcellular structures, an obvious next step for our platform, could deepen our understanding of lipid function in plant health and diseases.

Lipid engineering in plants is gaining importance in agriculture as lipids play essential roles as energy storage, cell membrane components, and signaling molecules in plant growth and defense mechanisms (Mamode Cassim and Mongrand, 2019; Raczyk and Rudzińska, 2015). In this study, we focused on three lipid-related genes (*WRI1*, *DGAT1* and *Oloesin*) and employed a classic push-pull-protection strategy (Vanhercke et al., 2019, 2014; Volk et al., 2023) to enhance lipid production through lipid engineering in cell systems. Following the overexpression of these three genes either individually or in a triple combination, using either the traditional strong promoter system or the more versatile CRISPR activation method, we observed a substantial increase in the accumulation of various types of fatty acids and lipids (Figures. 2-4). Notably, the increase observed in both TAG and phospholipids in cells transformed with *WRI1* was replicated in regenerated plants (Figure 3K). However, the push-pull-protect strategy resulted in plants with a much higher TAG content, but limited increases in phospholipid levels (Figure 3L). This illustrates the power of a combined cellular-level screening platform with rapid prototyping of transgenic regenerated plants. These results also have implications for the partitioning of carbon in cellular lipids between TAG and phospholipids. It appears that while *WRI1* expression alone acts to increase phospholipid species as well as TAG in leaf tissues of regenerated plants, the addition of *Oleosin* and *DGAT* acts to effectively “pull” and “protect” most of the extra lipids in the form of TAG, implying that the pools of DAG that lead to these products are connected (Chapman and Ohlrogge, 2012). The results indicate that our cell systems, including protoplasts and callus suspension cells, as well as our three automated workflows, are well suited for the prototyping of lipid metabolic engineering strategies. In addition, besides these three genes, numerous other genes are involved in oil production in leaves (Vanhercke et al., 2014). Hence, we have the potential to stack or combine additional genes from these three steps (pull, push, and protection) with the aim of enhancing vegetative lipid production for bioenergy production in plants.

In recent years, worldwide interest in biofoundries has led to the establishment of facilities in many countries, including the United States (e.g., iBioFAB), South Korea (K-BIOFOUNDRY) and China (e.g., Advanced Biofoundry Shenzhen), leading to initiatives like the Global Biofoundry Alliance., promoting worldwide collaboration and

519 standardized practices. However, while most efforts focus on microbial, mammalian,
520 and in vitro systems, our work aims to address the lack of plant engineering
521 biofoundries. Here, we develop plant-focused automated design-build-test-learn cycle
522 pipelines adaptable to global biofoundry frameworks to demonstrate the potential of this
523 technology. We plan for these protocols to be accessible to plant researchers via both
524 access to our service facility (the NSF iBioFoundry at the University of Illinois at Urbana-
525 Champaign) and by providing our open-access protocols for individual laboratories to
526 apply on low-cost liquid handlers, which are now priced similarly to other standard
527 molecular biology laboratory instruments.

528 Further work is needed to fully realize the potential of plant biofoundries. Regenerating
529 entire plants from protoplasts is challenging, which is why we developed callus
530 workflows, but protoplast regeneration workflows would be preferable. Our workflow still
531 relies on manual transfer of genetically-engineered calli into shoot media, a procedure
532 that could be automated by integrating a tissue culture robot. We provide here a proof of
533 concept using two plant species (*N. benthamiana* and maize) and four genes (*HCF136,*
534 *WRI1, DGAT1, and Oleosin*). The workflow has the capacity for high-throughput
535 investigations of much larger numbers of genes, for example, a screen for metabolic
536 regulators of lipid content. By establishing and validating the high-throughput pipeline
537 presented here, our work lays a solid foundation for transitioning plant engineering
538 towards biofoundries and extending the reach and impact of researchers aiming for
539 impactful discoveries for the next generation of plant science.

540 In summary, the FAST-PB pipeline developed here has potential to transform genome
541 editing, metabolic engineering, and metabolite profiling in plants by expanding the toolkit
542 for trait discovery and manipulation by executing iterative design-build-test-learn cycles
543 in small cell cultures. This workflow streamlines discovery, characterization, and fine-
544 tuning of traits in highly scalable small cell cultures, leading to the regeneration of full
545 plants after the desired phenotypes have been optimized.

Materials and Methods

Plant materials and growth conditions

Nicotiana benthamiana and maize (*Zea mays*) B73 were grown in a Conviron growth chamber (Conviron, Winnipeg, Canada) at the University of Illinois with a 16-hour light and 8-hour dark photoperiod. The temperatures during the light and dark periods were 26 °C and 22 °C, respectively. The relative humidity was consistently maintained at 50% and the light intensity provided was 100 µmol m^{-2} sec^{-1}, measured as photosynthetic photon flux density.

N. benthamiana plants used for callus generation in this study were germinated on 1⁄2 Murashige & Skoog (MS) media plates (Murashige and Skoog, 1962) containing 2% sucrose under 16 h/8 h, 22 °C /18 °C, light/dark conditions with 100 µmol m^{-2} s^{-1} light intensity. Leaf explants (0.5 x 0.5) cm were excised from approximately 2-week-old plants using aseptic technique. Explants were subsequently placed on MS plates containing 30 g/L sucrose, 0.1 g/L myo-inositol, 0.18 g/L KH_2PO_4, 1 mg/L Thiamine, 0.11 mg/L 2,4 D, pH 5.8 to induce callus generation. The plates were kept under continuous light at 25 °C for 2 weeks, and the resulting calli were transferred and maintained under continuous light at 25 °C with a shaking speed of 120 rpm (An, 1985).

Plasmids used in this study

A0502: pMOD_A0502 (#91012, Addgene) for CRISPR knockout system in *N. benthamiana*, B2103: pMOD_B2013 (#91061, Addgene) for CRISPR knockout and activation systems in plants, C0000: pMOD_C0000 (#91081, Addgene) for CRISPR knockout and activation systems in plants, D100: pTRANS_100 (#91198, Addgene) for protoplast system, T230: pTRANS_230 (obtained from Dr. Voytas's lab (Čermák et al., 2017)) for callus system, A1510: pMOD_A1510 (#91036, Addgene) CRISPR knockout system in maize, A3701: pMOD_A3701 (#91052, Addgene) for CRISPR activation system in *N. benthamiana*, A4110: pMOD_A4110 (#91056, Addgene) CRISPR activation system in maize. The detailed of the above plasmids can be found in the previous study (Čermák et al., 2017) and in Supplementary Table S1. pMDC43 and pMDC43-OWD can be found in the previous publications (Zhai et al., 2021, 2017b) for use in the transformation of *N. benthamiana* callus suspension cells, and the details of

the plasmid sequences can be found in the Supplementary Materials 1-2. Binary vector pPTN1586 was constructed by GoldenBraid modular assembly (Sarrion-Perdigones et al., 2013). Each gene of interest was synthesized by GenScript Biotech (Piscataway, NJ) to be GoldenBraid-domesticated and codon-optimized for sorghum (*Sorghum bicolor*). Genes used in pPTN1586 are *Cuphea avigera* var. *pulcherrima DGAT1* (*CpuDGAT1*, ANN46862.1), sorghum *Wrinkled1* (SbWRI1, XP_002450194.1), sesame (*Sesamum orientale*) *oleosin* (SiOle, Q9XHP2.1), *Cuphea palustris thioesterase* (Thio14, AAC49180.1), and *Cuphea avigera var. pulcherrima class B lysophosphatidic acid acyltransferase* (CpuLPATB, ALM22873.1). One amino acid residue in *SbWRI1* was changed (K10R) for protein stability (Zhai et al., 2017a). pZP212 (pPTN1586C) served as an empty vector used as a control plasmid during the transfection of maize protoplast cells with pPTN1586. Maps for pPTN1586 and pZP212 (pPTN1586C) are provided in the Supplementary materials. pZP212 (Hajdukiewicz et al., 1994) (pPTN1586C) serves as an empty vector used as a control plasmid during the transfection of maize protoplast cells with pPTN1586. Detailed sequences of pPTN1586 and pZP212 can be found in the Supplementary Materials 3-4.

Automation methods and instruments

iBioFAB workflows were encoded into *Momentum* software (Thermo Scientific™, Waltham, MA, USA) (Enghiad et al., 2022), which coordinates instruments, controls the Thermo Fisher F5 robotic arm, and manages plate movement and tracking. The Beckman Coulter Echo 550 instrument (Beckman Coulter, Brea, CA, USA) was used for DNA cloning applications while all manipulations of plant cell cultures were performed on the Tecan Fluent 1080 robotic liquid handler (Tecan, Männedorf, Switzerland). The Tecan Fluent 1080 is equipped with a Pickolo (SciRobotics, Israel) colony picker. Incubation steps were carried out in a Thermo Fisher Cytomat 2C automated incubator and centrifugation was performed in an Agilent Microplate Centrifuge (Agilent, Santa Clara, CA, USA). Growth of *Agrobacterium* cell cultures was quantified using a Tecan Infinite plate reader. All instruments are integrated onto a single platform and movement between instruments was performed by the Thermo Fisher F5 robotic arm. A 3D model of the integrated iBioFAB platform and flowchart of all automated workflows can be found in Supplementary Figures S1 and S2.

Gene cloning, genomic DNA extraction and chlorophyll fluorescence measurement

Benchling software was used to generate CRISPR guide RNAs (gRNAs) for the *WRI1* gene (Maize: *Zm00001d037760; N. benthamiana: NbS00061229g0004*) and the *DGAT1* gene (Maize: *Zm00001d005016; N. benthamiana:* NbS00004767g0010. Additionally, CRISPR-P v2.0 (Lei et al., 2014) was employed to generate two gRNAs targeting *HCF136* gene (*N. benthamiana: NbS00049766g0015*). Plasmids containing gRNAs were cloned using the previously reported protocol (Čermák et al., 2017) and the detailed of protocol can be found in Supplementary Method 1, which was translated into an automation workflow (Supplementary Figure S1A). For assembly of B plasmid, a Beckman Coulter Echo 550 acoustic liquid handler was used to mix gRNA cassette PCR reactions, plasmid B and cloning reactions, then a Tecan Fluent was used to transform assembled plasmid B into *E. coli.* Next, plasmid B with two gRNA sequences was extracted from an overnight culture of *E. coli* using the Tecan Fluent, following our previously reported automated protocol (Enghiad et al., 2022). Sanger sequencing was employed to confirm B plasmids before subsequent assembly. A second round Golden Gate reaction was employed to assemble plasmid modules A, B with gRNAs, and C into the pTRANS backbone using the Echo 550 instrument again followed by transformation into *E. coli* using the Tecan Fluent. In summary, 15 vectors were cloned using FAST-PB pipeline are listed in Supplementary Table S1 and gRNAs and primers are listed in Supplementary Table S4.

Genomic DNA was isolated from plant cells using the Promega Wizard® SV 96 Genomic DNA Purification System (Promega Corporation, Madison, WI, USA) following the manufacturer's protocol using the Tecan Fluent (Supplementary Figure S2E). Subsequently, Tecan Fluent Flexible-Channel Arm (FCA) arm transferred 5 uL of the DNA extracts into a new 96-well plate for DNA measurements using the high-throughput Lunatic UV/Vis absorbance spectrometer Microfluidic system (Unchained Labs, Pleasan).

After transfection for 24 hours with *HCF136* in maize or *N. benthamiana*, we utilized the Tecan Infinite Plate reader on the iBioFAB platform to measure chlorophyll fluorescence after overnight dark incubation of cell culture. This measurement was performed by

setting the Excitation Wavelength to 650 nm and the Emission Wavelength to 675 nm. The output yielded two datasets: one representing the intensity of chlorophyll fluorescence and the other reflecting cell intensity, as indicated by A600 measurements. Subsequently, the final result value was calculated as the ratio of the intensity of chlorophyll fluorescence to cell intensity. Targeted deletions in *HCF136* were confirmed via PCR, capillary sequencing and Inference of CRISPR Edits (ICE) analysis (Conant et al., 2022).

Protoplast isolation and transfection

To isolate protoplasts from Maize B73, 30 leaves were collected from 14-day-old etiolated seedlings then sliced into pieces with 1 mm thickness and evenly distributed into a 24 square-well V-bottom plate. *N. benthamiana* protoplasts were isolated from five 8-week-old leaves cut into 2 mm thickness and distributed to another same type of plate. After slicing the leaves and distributing them into two 24-well plates (one for maize and the other for *N. benthamiana*), the remaining isolation steps were performed on the iBioFAB platform (Supplementary Figures S2C-D). First, the FCA arm of Tecan Fluent distributed 2 mL of enzyme solution into each well of a 24-well plate followed by shaking for four hours at 100 RPM at room temperature without light in the incubator of the Tecan Fluent. Next, the digested leaf solution was filtered on a 24-well AcroPrep filter plate with 30-40 µm pore volume (Pall Corporation, Port Washington, New York, USA) using the Te-VacS vacuum separation module integrated into the Tecan Fluent system. The filtered solution was then centrifuged on an Agilent automated microplate centrifuge (Agilent, Santa Clara, CA, USA) for 2 min at 150 rcf. The Tecan Fluent was again used to remove the supernatant and wash cells by adding 200 µL of W5 solution to each well. Following another round of centrifugation and supernatant removal, the cells were resuspended into 200 µL of W5 solution. All cells from all 24 wells were then combined into a single tube and centrifuged again. After supernatant removal, the cells were resuspended into 5 mL of MMG solution using the FCA arm, and the cell concentration was determined using a hemocytometer (Thermo Scientific, Waltham, MA, USA).

Next, the FCA arm slowly distributed 100 µL of isolated protoplasts into each well of a 96-well plate. To optimize transfection efficiency, three different average number

molecular weights of PEG (2050, 3350, and 4000) were used: PEG 2050 (Sigma-Aldrich, Lot #: BCBW7040), PEG 3350 (Sigma-Aldrich, Lot #: MKCL5061), and PEG 4000 (Sigma-Aldrich, Lot #: BCCF2031). These three types of PEG and one type of plasmid p201GFP-Cas9 (Jacobs et al., 2015) were gently added into each well of 96-well plate containing protoplast cells and then slowly mixing them, according to a predefined worklist using the Momentum™ software. The transformation mixtures were incubated in the dark at room temperature for 30 min. Subsequently, the FCA arm added 600 µL of W5 solution to each well and mixed gently to stop the transformation reaction. The F5 robotic arm moved the plate to the centrifuge followed by centrifugation for 2 min at 150 rcf (Relative Centrifugal Field) and then removal of supernatants and resuspension into fresh W5 solution. After second wash, plates were centrifuged again for 2 min at 150 rcf and cells were resuspended into 100 µL of W5 solution through using the Tecan Fluent system. After determining that PEG 2050 yielded the highest transfection efficiency, we used this optimal PEG type to transfect cells in both maize B73 and *N. benthamiana*. All automated transfection procedures with same PEG type 2050 but different plasmids were conducted as previously described. In maize B73, we employed eight types of plasmids (A4110, A4110-DGAT1, A4110-WRI1, pPTN1586C, pPTN1586, A1510, A1510-HCF136, p201GFP-Cas9 (Jacobs et al., 2015)), with each type having four to ten replicates. Similarly, *for N. benthamiana* transfection, we used six types of plasmids (P-A3701, P-A3701-DGAT1, P-A3701-WRI1, P-A0502, P-A0502-HCF136, p201GFP-Cas9), also with four to ten replicates for each type.

***N. benthamiana* callus transformation and whole-plant regeneration**

Two seven-week-old calli were placed in a single well of a 6-well plate, resulting in two calli per well, for a total of two 6-well plates. Tecan Fluent was used to add 3 mL MS liquid media to each well. The plates were then exposed to continuous light for a period of 20 days while shaking at 200 rpm (Revolutions Per Minute). Prior to transformation, the Pickolo colony picker (SciRobotics, Kfar Saba, HaMerkaz, Israel) was used to pick *Agrobacterium tumefaciens* colonies from an agar plate containing rifampicin and kanamycin antibiotics into a 96-deepwell plate containing 1 mL LB media per well. Specifically, seven colonies were selected from seven different plates, namely C-A3701, C-A3701-WRI1, C-A3701-DGAT1, C-A1510, C-A1510-HCF136, pMDC43, and

pMDC43-OWD. The F5 robotic arm transferred the plate to the Thermo Scientific™ Cytomat™_6K automated incubator (Thermo Scientific, Waltham, MA, USA), where it underwent overnight outgrowth at 200 rpm. The following day, the 96-deep well plate was taken out from the incubator and placed on the dock of the Tecan Fluent. Subsequently, the FCA arm of the Tecan Fluent transferred 100 µl of the overnight culture to a new 96-well plate for optical density (OD) measurement at 600 nm using Tecan infinite plate reader (Männedorf, Switzerland) on the iBioFAB platform. Following the OD measurement, if the OD of the cell culture was within the range of 0.4-1, the optimal overnight culture was introduced to the ten-week-old callus suspension cells in the 6-well plates. The co-culture was conducted under light conditions for two days. Next, co-culture cells were washed four times with MS liquid media using the Tecan Fluent. After washing, calli transformed with C-A3701, C-A3701-WRI1, C-A3701-DGAT1, C-A1510 and C-A1510-HCF136 were placed on 2 mg/L phosphinothricin (PPT) selection MS media plates, while those transformed with pMDC43 and pMDC43-OWD were placed on a 15 mg/L hygromycin-selected MS media plates. The automated procedures are demonstrated in Supplementary Figure S2B. Shoot and root regeneration procedures followed those described in a previous study (Clemente, 2006). Briefly, genetically engineered calli were transferred into the shoot media (MS Salts & MS vitamins + 30 g sucrose + 2 mg/L kinetin + 1 mg/L IAA (auxin)+ 400 mg/L timentin + 2.0 mg/L glufosinate ammonium- for bar gene selection- or 20 mg/L hygromycin selection). After 10-16 weeks, shoots were generated then transferred to the root media (MS salts & vitamins + 30g sucrose+ 200 mg/L timentin + 2.0 mg/L glufosinate ammonium- for bar gene selection- or 20 mg/L hygromycin selection- for rooting). After 5-8 weeks, fully rooted plants were transferred to pots with PRO-MIX BX BIOFUNGICIDE MYCORRHIZAE soil in the growth chamber.

RNA extraction and RT-qPCR analysis

RNA was extracted from callus and protoplast cultures using the ZR Plant RNA Miniprep™ kit (R2024, Zymo Research, CA, USA) and TRIzol™ Reagent (15596026, Thermo Scientific, Waltham, Massachusetts, USA), respectively. The single-stranded cDNA was synthesized using the High-Capacity cDNA Reverse Transcription Kit (ThermoFisher Scientific; Waltham, Massachusetts, USA). Real-time PCR (qPCR) was

performed using the Power SYBR® Green PCR Master Mix (ThermoFisher Scientific) in a LightCycler 480 instrument (Roche; Indianapolis, IN, USA). Gene expression levels were normalized to the expression of the constitutively expressed reference genes (Table S4). Relative gene expression was calculated following previously published methods (Livak and Schmittgen, 2001; Dong et al., 2020). The qPCR primers are shown in Supplementary Table S4.

Lipid extraction and LC-MS/MS analysis

Lipid extraction from plant tissues and protoplasts were performed as described elsewhere (Zhai et al., 2018). Briefly, 700 µL of extraction solvent (chloroform: methanol: formic acid 2:1:0.1 v/v/v) and 350 µL of 1M KCl with 0.2M H_3PO_4 were added for liquid-liquid partition. This was vortexed for 30 min, centrifuged at 20,000 x g for 10 min, then the lower layer was taken and dried using a SpeedVac vacuum concentrator (Thermo Scientific, USA). The samples were redissolved in 200 µL of an LC-MS grade solvent mixture of isopropanol/acetonitrile/water 65/30/5, added to an HPCL vial insert, and 2 µL SPLASH™ LIPIDOMIX® Mass Spec Standard (Avanti Polar Lipids was added to each of the samples for an internal calibrant.

LC-MS/MS analysis was performed on a Vanquish™ UHPLC coupled with Q Exactive™ Orbitrap Mass Spectrometer (Thermo Scientific, USA) with HESI source. An Acquity UPLC® BEH C18 column (2.1 × 100 mm, 1.7 µm) was kept at 45 ºC. Solvent A was 60:40 (v/v) acetonitrile:water with 10 mM ammonium formate and 0.1 % formic acid, and solvent B was 90:10 (v/v) isopropanol:acetonitrile with 10 mM ammonium formate and 0.1 % formic acid. The gradient started with 15% phase B and increased to 50% at 2 min, then to 98% at 15.5 min. The column was washed at 98% phase B for 2 min, and continued with equilibration using 15% B from 17.6 to 20 min. Flow rate was kept at 250 µl/min.

For mass spectrometry analysis, the capillary temperature was set at 300 ºC, for both positive and negative modes. Sheath gas flow rate was set to 35 and aux gas to 10. For positive scan, the spray voltage was 3.5 kV and for negative was 2.8 kV. Positive and negative data were collected by separate injections. Data was acquired by full MS scan followed by data dependent scans with fragmentation energy. Full MS scan range was *m/z* 150-1500. The AGC (Automatic Gain Control) target was set to 3e6. For data

dependent MS^2, the top 10 ions were selected for fragmentation at stepped normalized collision energy of 15, 25 and 35. The isolation window was *m/z* 1.0, resolution was set to 17,500, the AGC target was at $1e^5$, and dynamic exclusion was set as 5.0 s for triggered ions. Centroid mode was used for all data collection. Peak detection, alignment, and identification were performed on MS-Dial (ver 4.90) with built-in *in silico* LC/MS/MS based lipidomics database (Tsugawa et al., 2020). Identification was based on MS2 match, and the score cut off was set at 80%. For lipid quantification, the average peak area of each class of lipid was normalized using internal standards (SPLASHTM LIPIDOMIX® Mass Spec Standard, Avanti Polar Lipids, Alabaster, Alabama, USA) then divided by the respective sample fresh weight (callus tissue or leaf) or by the total number of cells analyzed (protoplast cells).

Gas chromatography-mass spectrometry (GC-MS) analysis

Qualitative, targeted fatty acids analysis was performed using an Agilent 6890N gas chromatography attached to a 5975B MS in the Metabolomics Laboratory of Roy J. Carver Biotechnology Center, University of Illinois at Urbana-Champaign, as previously described (Xue et al., 2020). One microliter injection of the sample was made into the column in a Pulsed Splitless mode, with the front inlet pressure elevated to 40 psi for 18 s. Helium was the carrier gas used. The front inlet, MS transfer line, MS source, and MS quad were maintained at 300 ºC, 230 ºC, 230 ºC and 150 ºC, respectively. The GC oven temperature protocol was as follows: 50 ºC for 2 min, ramp up at 30 ºC/min for a 2 min hold at 120 ºC, a second ramp up at 30 ºC/min for a 2 min hold at 180 ºC, and a final ramp up at 30 ºC/min for a 9.33 min hold at 250°C. For fatty acids quantification, the average peak area of each type of fatty acid was normalized using an internal standard (Tricosanoic acid, C23:0) then divided by the fresh weight of callus tissue.

Matrix application and high-throughput MALDI-MS analysis

A matrix solution containing 45 mg/mL 2,5-dihydroxybenzoic acid dissolved in 70% methanol was deposited onto ITO-coated microscopy slides using an HTX M5-Sprayer (HTX Technologies). The sprayer temperature was set to 70 ºC, with a flow rate of 0.1 ml min^{-1}, track spacing of 3 mm, pressure of 10 psi, and a gas flow rate of 3 l min^{-1}. One pass of the matrix was applied to the slides, with a final matrix density of 3.195 mg/mm^2.

MALDI-MS analysis was performed with a SolariX XR 7T FT-ICR mass spectrometer (mass spectrometer equipped with an APOLLO II dual MALDI/ESI source (Bruker). Data were acquired in positive-mode with a mass range of *m/z* 54-1,600, yielding a transient length of 0.524 s using a Smartbeam-II UV laser (355 nm) set to "Small" mode, generating a ~100-µm diameter laser footprint. Each MALDI-MS acquisition consisted of 500 laser shots at a frequency of 1,000 Hz. microMS was used as previously described to generate instrument stage coordinates and geometry files for all MALDI acquisitions of selected protoplasts with a distance filter of 200 µm (removed protoplasts located closer than 200 µm to each other from the target list) (Comi et al., 2017). Peak picking and peak export were performed using Compass DataAnalysis 4.4 (Bruker) with a signal-to-noise ratio or 5 and a relative intensity threshold of 0.01%. Mass spectral binning was performed in custom Matlab scripts with a semicontinuous bin width of 3 ppm. Features were mass matched to a bulk LC-MS/MS database using a 5 ppm filter, and cells with fewer than 5 matched lipids were removed from the sample set.

Thin layer chromatography (TLC), lipid staining and visualization of oil droplets

TLC was performed following a previous study (Zhang et al., 2016). Briefly, after lipid extraction, we loaded 15 µL of standards and 25 µL of lipid extract samples onto the TLC plate. After a 45-minute run, TLC was visualized through ionization. Lipid staining and visualization of oil droplets followed the method described in a previous study (Cai et al., 2015) using leaves from three-month-old genetically engineered *N. benthamiana*.

Statistical methods in this study

MALDI-MS data was analyzed using a two-tailed Mann-Whitney test. All other P-values provided were generated using the two-tailed Welch's t-test unless otherwise stated. Asterisks indicate: ****$P < 0.0001$; ***$P < 0.001$; **$P < 0.01$; *$P < 0.05$. Statistical analysis, including volcano plot analysis, was conducted using the web tool available at https://www.metaboanalyst.ca/ (Lu et al., 2023).

Accession Numbers

Information on all the genes can be found in Supplementary Table S4.

Funding

We acknowledge the Center for Advanced Bioenergy and Bioproducts Innovation (U.S. Department of Energy, Office of Science, Office of Biological and Environmental Research under Award Number DE- SC0018420). Any opinions, findings, and conclusions or recommendations expressed in this publication are those of the author(s) and do not necessarily reflect the views of the U.S. Department of Energy. The funders had no role in study design, data collection and analysis, decision to publish, or preparation of the manuscript.

Acknowledgments

We express our gratitude to Benjamin Haas for generously sharing the gene cloning protocol and reference primers for RT-qPCR, which greatly contributed to the success of this study. We also extend our thanks to Dr. Thomas Clemente for providing the necessary information on plasmids (pPTN1586C and pPTN1586), which were instrumental in advancing our research. We would like to acknowledge Dr. Zhiyang Zhan and Dr. Yingqi Cai for providing the plasmids (pMDC43 and pMDC43-OWD). We thank Dr. Kingsley Boateng and Dr. Austin Cyphersmith for their assistance in setting up the microscopy procedure.

Author contributions

All authors designed experiments, analyzed data, and assisted in the writing and editorial process. J.D., S.W.C., S.L., D.C.C., J.B., S.Z., K.P., M.R. performed the experiments. S.B., E.C., J.S., H.Z., J.V.S., and M.E.H. conceived and supervised the overall project.

Competing interests

All authors declare no competing interests.

Figure Legends

Figure 1. Overview of the FAST-PB for high-throughput genome editing and lipid engineering in protoplast and callus cell systems. (**A**) Automated gene cloning using the Golden Gate cloning method streamlines the process of plasmid assembly (Design). (**B**) Automated callus transformation with CRISPR vectors or strong promoter vectors to facilitate plant regeneration with the increased lipid production trait. GFP fluorescence indicates successful transformation (Build). (**C**) Automated protoplast isolation and transfection (Build). (**D**) Top: Protoplast cells from transgenic callus tissues applied on MALDI slides for lipid measurement and LC-MS analysis of lipids from callus

and protoplast cells. Bottom: Characterization of lipids through MALDI spectra analysis and lipid class quantification (Test).

Figure 2. Automated protoplast isolation and transfection to genotyping and phenotyping cells. (**A**) Protoplast isolation from *N. benthamiana* leaves (left) using automation yielded abundant and high-quality protoplast cells (pictured at 40x magnification, middle). Protoplasts transfected with the Cas9 vector (p201GFP-Cas9) exhibit GFP fluorescence (right). (**B**) Etiolated maize B73 (left) allowed successful protoplast isolation on the automation platform, yielding abundant high-quality protoplast cells (pictured at 40x magnification, middle). Subsequent transfection with the Cas9 vector (p201GFP-Cas9) induced GFP fluorescence in numerous cells (right). (**C**) Total intact cell number was counted under three types of PEG (2050, 3350, 4000) treatments in the etiolated maize B73 and *N. benthamiana*. Biological replicate n = 4. (**D**) Transfection efficiency (Ratio of GFP-expressing and total intact cell numbers) in four days after transfection. Biological replicate n = 4. For C and D, Center line represents the median of the data. Box limits Indicate the upper and lower quartiles (25th and 75th percentiles). Whiskers extend to 1.5 times the interquartile range (IQR) from the upper and lower quartiles. Points represent outliers, which are data points beyond the whiskers. (**E**) Quantification of chlorophyll fluorescence intensity following *HCF136* gene knockout (HCF136-KO) in both maize and *N. benthamiana*. n = 10. (**F**) Mutation analysis of the *HCF136* gene performed using next-generation Sanger sequencing and Inference of CRISPR Editing (ICE) analysis (Hsiau et al., 2018; Dong et al., 2020) in maize and *N. benthamiana*. A DNA sequence alignment is shown where the first line of the alignment shows control sequence from unedited cells. The vertical dotted line shows the target site of the guide RNA. Subsequent sequences show dashes where bases have been deleted at the target site relative to the reference line. (**G**) Lipid classes were measured across four days in protoplasts using LC-MS/MS in *N. benthamiana* (top) and etiolated maize B73 (bottom). Biological replicate n = 6. (**H**) Top: Lipid analysis and quantification after overexpression of P-3701-WRI1 (3701-WRI1) and P-3701-DGAT (3701-DGAT1) through using the CRISPR activation system, with P-3701 (3701) as a control in *N. benthamiana*. Biological replicate n = 4. Bottom: Lipid analysis and quantification after overexpression of lipid-related genes in etiolated maize

B73. Two groups in this study, first group is 4110, 4110-WRI1, and 4110-DGAT using the CRISPR activation system, and 4110 as a control; the second group is pPTN1586 and pPTN1586C, and this group refers to a positive control group using the strong promoter system. pPTN1586 contains five genes (*DGAT1, WRI1, Oleosin, Thio14,* and *LPATB*) for overexpression, with pPTN1586C serving as an empty vector control for pPTN1586. Biological replicate n = 5. For lipid quantification, the average peak area of each class of lipid was normalized using internal standards then divided by the total number of protoplast cells analyzed. Error bars represent standard error. Asterisks indicate: ***$P < 0.001$; **$P < 0.01$; *$P < 0.05$, calculated using two-tailed Welch's t-test. TAG: Triacylglycerol; DAG: Diacylglycerol; PC: Phosphatidylcholine; PE: Phosphatidylethanolamine; PA: Phosphatidic acid; PG: Phosphatidylglycerol; PI: Phosphatidylinositol; PS: Phosphatidylserine; LPC: Lysophosphatidylcholine; LPE: Lysophosphatidylethanolamine.

Figure 3. Lipid profiling and comparative analysis of genetically engineered *N. benthamiana* callus and leaf samples using LC-MS/MS. A-C, Annotated volcano plots (log2(FC) versus -log10(P-values) showing the up- and down-regulated lipid species in callus cultures after (**A**) simultaneous overexpression of (OWD) genes using the strong 35S promoter, 43 as a control (**B**) overexpression of *WRI1* using CRISPR activation, 3701 as a control, and (**C**) overexpression of DGAT1 using CRISPR activation, 3701 as a control. n >= 3. **D-F**, Quantification of lipid classes through fold change calculation for the overexpression of *WRI1*, *DGAT1* and *Oleosin* genes (**D**), overexpression of the *WRI1* gene (**E**), and overexpression of the *DGAT1* gene (**F**). n >= 3. **G-I**, Fatty acids quantification through fold change formula for overexpression of *WRI1*, *DGAT1* and *Oleosin* genes (**G**), the *WRI1* gene (**H**), the *DGAT1* gene (**I**). n >= 3. Biological replicate n = 3 for the OWD group. **J**, Genetically engineered calli and plants. The images show the growth and characteristics of genetically engineered calli and plants transformed with pMDC43 as a control and pMDC43-OWD vectors. (Top Left) Callus tissues generated from the pMDC43-OWD vector, which overexpresses *Oleosin*, *WRI1*, and *DGAT1* (OWD) genes, grown on MS medium containing hygromycin for resistance selection. (Top Right) Fluorescence image of pMDC43-OWD callus tissues, indicating successful genetic transformation with visible green fluorescence. (Bottom

Left) Regenerated plant from the pMDC43 vector. (Bottom Right) Regenerated plant from the pMDC43-OWD vector. Scale bars represent 10 mm. **K**, Lipid profiling in one-month-old genetically engineered *N. benthamiana* after overexpression of *WRI1* (3701-WRI1) using the CRISPR activation system. The sample size is n = 3, representing independent genetically engineered plants. **L**, Lipid profiling in one-month-old genetically engineered *N. benthamiana* after overexpression of *Oleosin*, *WRI1* and *DGAT1* (pMDC43-OWD). The sample size is n > 3, representing independent genetically engineered plants. Dots on bar charts represent the means of replicated measurements of individual genetically engineering events. For lipid quantification, the average peak area of each class of lipid was normalized using internal standards then divided by the respective sample fresh weight (callus tissue or leaf). Error bars represent standard error. Asterisks indicate: ***P < 0.001; **P < 0.01; *P < 0.05, calculated using a two-sided t-test for the volcano plots (**A-C**) and two-tailed Welch's t-test for the remaining figures (**D-L**). TAG: Triacylglycerol; DAG: Diacylglycerol; PC: Phosphatidylcholine; PE: Phosphatidylethanolamine; PA: Phosphatidic acid; PG: Phosphatidylglycerol; PI: Phosphatidylinositol; PS: Phosphatidylserine; LPC: Lysophosphatidylcholine; LPE: Lysophosphatidylethanolamine.

Figure 4. Lipidomic analysis of genetically engineered callus-derived protoplast samples using LC-MS/MS and high-throughput single-cell measurements via MALDI FT-ICR MS. (**A**) Protoplast cells in the W5 liquid media were imaged to check the quality before performing MALDI/MS (on the left). Then, using Hoechst staining method to stain the cells, they were imaged (on the right). (**B**) Overview of the single-cell MALDI-MS workflow for callus-derived protoplasts. (**C**) Mass spectra with identified lipid species annotated in the wildtype calli-derived protoplast. (**D**) Lipid profiling in callus-derived protoplast cells. n = 6. (**E**) Ranked dot plot showing the top ten lipid features for the control (43) and genetically engineered (43-OWD) protoplast samples. Samples are colored by their p-value-modulated z score and the size of each dot represents the fraction of the total samples that had each feature. (**F**) Subtracted average mass spectra for control (43) and genetically overexpressed (43-OWD) protoplasts across the entire lipid range. The accurate *m/z* values for can be found in Supplementary Table S2. (**G**) Selected *m/z* window around the TAG lipid region, with

detected lipid species annotated. The accurate *m/z* values for can be found in Supplementary Table S2. (**H**) Comparison of lipid class between the LC-MS/MS and MALDI-MS datasets. (**I**) The comparison of TAG lipid features between LC-MS/MS and single-cell MALDI-MS detection. Biological replicate n > = 3 for all MALDI-MS and LC-MS/MS datasets. Error bars represent standard error. Asterisks indicate: ****$P < 0.0001$; ***$P < 0.001$; **$P < 0.01$; *$P < 0.05$, LCMS statistics were calculated using a two-tailed Welch's t-test and MALDI-MS data was analyzed using a two-tailed Mann-Whitney test. TAG: Triacylglycerol; DAG: Diacylglycerol; PC: Phosphatidylcholine; PE: Phosphatidylethanolamine; PA: Phosphatidic acid; PG: Phosphatidylglycerol; PI: Phosphatidylinositol; PS: Phosphatidylserine; LPC: Lysophosphatidylcholine; LPE: Lysophosphatidylethanolamine.

References

Ali, A., Abouleila, Y., Shimizu, Y., Hiyama, E., Emara, S., Mashaghi, A., and Hankemeier, T. (2019). Single-cell metabolomics by mass spectrometry: Advances, challenges, and future applications. TrAC - Trends Anal. Chem. **120**.

An, G. (1985). High Efficiency Transformation of Cultured Tobacco Cells. Plant Physiol. **79**.

Bourceau, P., Geier, B., Suerdieck, V., Bien, T., Soltwisch, J., Dreisewerd, K., and Liebeke, M. (2023). Visualization of metabolites and microbes at high spatial resolution using MALDI mass spectrometry imaging and in situ fluorescence labeling. Nat. Protoc.

Cai, Y., Goodman, J.M., Pyc, M., Mullen, R.T., Dyer, J.M., and Chapmana, K.D. (2015). Arabidopsis SEIPIN proteins modulate triacylglycerol accumulation and influence lipid droplet proliferation. Plant Cell **27**.

Castro, D.C., Chan-Andersen, P., Romanova, E. V., and Sweedler, J. V. (2023). Probe-based mass spectrometry approaches for single-cell and single-organelle measurements. Mass Spectrom. Rev.

Castro, D.C., Xie, Y.R., Rubakhin, S.S., Romanova, E. V., and Sweedler, J. V. (2021). Image-guided MALDI mass spectrometry for high-throughput single-organelle characterization. Nat. Methods **18**.

Čermák, T., Curtin, S.J., Gil-Humanes, J., Čegan, R., Kono, T.J.Y., Konečná, E., Belanto, J.J., Starker, C.G., Mathre, J.W., Greenstein, R.L., and Voytas, D.F. (2017). A multipurpose toolkit to enable advanced genome engineering in plants. Plant Cell **29**.

Chao, R., Mishra, S., Si, T., and Zhao, H. (2017). Engineering biological systems using automated biofoundries. Metab. Eng. **42**.

Chapman, K.D. and Ohlrogge, J.B. (2012). Compartmentation of triacylglycerol accumulation in plants. J. Biol. Chem. **287**.

Clemente, T. (2006). *Nicotiana* (*Nicotiana tobaccum, Nicotiana benthamiana*). In Agrobacterium Protocols.

Cole, B. et al. (2021). Plant single-cell solutions for energy and the environment. Commun. Biol. **4**.

Comi, T.J., Neumann, E.K., Do, T.D., and Sweedler, J. V. (2017). microMS: A Python Platform for Image-Guided Mass Spectrometry Profiling. J. Am. Soc. Mass Spectrom. **28**.

Conant, D., Hsiau, T., Rossi, N., Oki, J., Maures, T., Waite, K., Yang, J., Joshi, S., Kelso, R., Holden, K., Enzmann, B.L., and Stoner, R. (2022). Inference of CRISPR Edits from Sanger Trace Data. Cris. J. **5**.

Cui, Y., Gao, J., He, Y., and Jiang, L. (2020). Plant extracellular vesicles. Protoplasma **257**.

Demirer, G.S., Zhang, H., Matos, J.L., Goh, N.S., Cunningham, F.J., Sung, Y., Chang, R., Aditham, A.J., Chio, L., Cho, M.J., Staskawicz, B., and Landry, M.P. (2019). High aspect ratio nanomaterials enable delivery of functional genetic material without DNA integration in mature plants. Nat. Nanotechnol. **14**.

Dong, J., Zielinski, R.E., and Hudson, M.E. (2020). t-SNAREs Bind the Rhg1 α-SNAP and Mediate Soybean Cyst Nematode Resistance. Plant J. cell Mol. Biol.

Eberwine, J. et al. (2023). Subcellular omics: a new frontier pushing the limits of resolution, complexity and throughput. Nat. Methods **20**.

Enghiad, B., Xue, P., Singh, N., Boob, A.G., Shi, C., Petrov, V.A., Liu, R., Peri, S.S., Lane, S.T., Gaither, E.D., and Zhao, H. (2022). PlasmidMaker is a versatile, automated, and high throughput end-to-end platform for plasmid construction. Nat. Commun. **13**.

Guo, S., Zhang, C., and Le, A. (2021). The limitless applications of single-cell metabolomics. Curr. Opin. Biotechnol. **71**.

Hajdukiewicz, P., Svab, Z., and Maliga, P. (1994). The small, versatile pPZP family of Agrobacterium binary vectors for plant transformation. Plant Mol. Biol. **25**.

Hillson, N. et al. (2019). Building a global alliance of biofoundries. Nat. Commun. **10**.

Hsiau, T., Maures, T., Waite, K., Yang, J., Kelso, R., Holden, K., and Stoner, R. (2018). Inference of CRISPR Edits from Sanger Trace Data. bioRxiv: 251082.

Huang, Y., Shang, M., Liu, T., and Wang, K. (2022). High-throughput methods for genome editing: The more the better. Plant Physiol. **188**.

Ikeuchi, M., Sugimoto, K., and Iwase, A. (2013). Plant callus: Mechanisms of induction and repression. Plant Cell **25**.

Jacobs, T.B., LaFayette, P.R., Schmitz, R.J., and Parrott, W.A. (2015). Targeted genome modifications in soybean with CRISPR/Cas9. BMC Biotechnol. **15**.

Karlson, C.K.S., Mohd-noor, S.N., Nolte, N., and Tan, B.C. (2021). Crispr/dcas9-based systems: Mechanisms and applications in plant sciences. Plants **10**.

Lawson, D.A. et al. (2015). Single-cell analysis reveals a stem-cell program in human metastatic breast cancer cells. Nature **526**.

Lei, Y., Lu, L., Liu, H.Y., Li, S., Xing, F., and Chen, L.L. (2014). CRISPR-P: A web tool for synthetic single-guide RNA design of CRISPR-system in plants. Mol. Plant **7**: 1494–1496.

Lenaghan, S.C. and Neal Stewart, C. (2019). An automated protoplast transformation system. In Methods in Molecular Biology.

Liu, D., Shi, L., Han, C., Yu, J., Li, D., and Zhang, Y. (2012). Validation of Reference Genes for Gene Expression Studies in Virus-Infected Nicotiana benthamiana Using Quantitative Real-Time PCR. PLoS One **7**.

Livak, K.J. and Schmittgen, T.D. (2001). Analysis of relative gene expression data using real-time quantitative PCR and the 2-ΔΔCT method. Methods **25**: 402–408.

Lu, Y., Pang, Z., and Xia, J. (2023). Comprehensive investigation of pathway enrichment methods for functional interpretation of LC-MS global metabolomics data. Brief. Bioinform. **24**.

Maitra, S., Viswanathan, M.B., Park, K., Kannan, B., Alfanar, S.C., McCoy, S.M., Cahoon, E.B., Altpeter, F., Leakey, A.D.B., and Singh, V. (2022). Bioprocessing, Recovery, and Mass Balance of Vegetative Lipids from Metabolically Engineered “oilcane” Demonstrates Its Potential as an Alternative Feedstock for Drop-In Fuel Production. ACS Sustain. Chem. Eng. **10**.

Mamode Cassim, A. and Mongrand, S. (2019). Lipids light up in plant membranes. Nat. Plants **5**.

Manoli, A., Sturaro, A., Trevisan, S., Quaggiotti, S., and Nonis, A. (2012). Evaluation of candidate reference genes for qPCR in maize. J. Plant Physiol. **169**.

Martín-Saiz, L. et al. (2023). Using the Synergy between HPLC-MS and MALDI-MS Imaging to Explore the Lipidomics of Clear Cell Renal Cell Carcinoma. Anal. Chem. **95**.

Meurer, J., Plücken, H., Kowallik, K. V., and Westhoff, P. (1998). A nuclear-encoded protein of prokaryotic origin is essential for the stability of photosystem II in Arabidopsis thaliana. EMBO J. **17**.

Mumm, R.H. (2013). A look at product development with genetically modified crops: Examples from maize. J. Agric. Food Chem. **61**.

Murashige, T. and Skoog, F. (1962). A Revised Medium for Rapid Growth and Bio Assays with Tobacco Tissue Cultures. Physiol. Plant. **15**.

Napier, J.A., Haslam, R.P., Beaudoin, F., and Cahoon, E.B. (2014). Understanding and manipulating plant lipid composition: Metabolic engineering leads the way. Curr. Opin. Plant Biol. **19**.

Neumann, E.K., Do, T.D., Comi, T.J., and Sweedler, J. V. (2019). Exploring the Fundamental Structures of Life: Non-Targeted, Chemical Analysis of Single Cells and Subcellular Structures. Angew. Chemie - Int. Ed. **58**.

Norouzi, O., Hesami, M., Pepe, M., Dutta, A., and Jones, A.M.P. (2022). In vitro plant tissue culture as the fifth generation of bioenergy. Sci. Rep. **12**.

Pandian, K., Matsui, M., Hankemeier, T., Ali, A., and Okubo-Kurihara, E. (2023). Advances in single-cell metabolomics to unravel cellular heterogeneity in plant biology. Plant Physiol.

Raczyk, M. and Rudzińska, M. (2015). Analysis of plant lipids. Plant Lipids Sci. Technol. Nutr. Value Benefits to Hum. Heal. **661**.

Rigoulot, S.B. et al. (2023). Automated, High-Throughput Protoplast Transfection for Gene Editing and Transgene Expression Studies. In Plant Genome Engineering. Methods in Molecular Biology, S.B. Rigoulot, ed (Humana, New York, NY.), pp. 129–149.

Roy, A.L., Conroy, R., Smith, J., Yao, Y., Beckel-Mitchener, A.C., Anderson, J.M., and Wilder, E.L. (2018). Accelerating a paradigm shift: The common fund single cell analysis program. Sci. Adv. **4**.

Sarrion-Perdigones, A., Vazquez-Vilar, M., Palací, J., Castelijns, B., Forment, J., Ziarsolo, P., Blanca, J., Granell, A., and Orzaez, D. (2013). Goldenbraid 2.0: A comprehensive DNA assembly framework for plant synthetic biology. Plant Physiol. **162**.

Seydel, C. (2021). Single-cell metabolomics hits its stride. Nat. Methods **18**.

Si, T., Chao, R., Min, Y., Wu, Y., Ren, W., and Zhao, H. (2017). Automated multiplex genome-scale engineering in yeast. Nat. Commun.

Si, T., Xiao, H., and Zhao, H. (2015). Rapid prototyping of microbial cell factories via genome-scale engineering. Biotechnol. Adv. **33**.

Squire, H.J., Tomatz, S., Voke, E., González-Grandío, E., and Landry, M. (2023). The emerging role of nanotechnology in plant genetic engineering. Nat. Rev. Bioeng. **1**.

Taylor, M.J., Lukowski, J.K., and Anderton, C.R. (2021). Spatially Resolved Mass Spectrometry at the Single Cell: Recent Innovations in Proteomics and Metabolomics. J. Am. Soc. Mass Spectrom. **32**.

TSAI, C.H., WEN, M.C., and KINSELLA, J.E. (1982). Cocobean Tissue Culture: Lipid Composition and Fatty Acid Metabolism. J. Food Sci. **47**.

Tsugawa, H. et al. (2020). A lipidome atlas in MS-DIAL 4. Nat. Biotechnol. **38**.

Urzì, O., Raimondo, S., and Alessandro, R. (2021). Extracellular vesicles from plants: Current knowledge and open questions. Int. J. Mol. Sci. **22**.

Vanhercke, T. et al. (2014). Metabolic engineering of biomass for high energy density: Oilseed-like triacylglycerol yields from plant leaves. Plant Biotechnol. J. **12**.

Vanhercke, T., Dyer, J.M., Mullen, R.T., Kilaru, A., Rahman, M.M., Petrie, J.R., Green, A.G., Yurchenko, O., and Singh, S.P. (2019). Metabolic engineering for enhanced oil in biomass. Prog. Lipid Res. **74**.

Volk, M.J., Tran, V.G., Tan, S.I., Mishra, S., Fatma, Z., Boob, A., Li, H., Xue, P., Martin, T.A., and Zhao, H. (2023). Metabolic Engineering: Methodologies and Applications. Chem. Rev. **123**.

Xue, P., Si, T., Mishra, S., Zhang, L., Choe, K., Sweedler, J. V., and Zhao, H. (2020). A mass spectrometry-based high-throughput screening method for engineering fatty acid synthases with improved production of medium-chain fatty acids. Biotechnol. Bioeng. **117**.

Yin, K., Gao, C., and Qiu, J.L. (2017). Progress and prospects in plant genome editing. Nat. Plants **3**.

Zhai, Z., Keereetaweep, J., Liu, H., Feil, R., Lunn, J.E., and Shanklin, J. (2018).

Trehalose 6-phosphate positively regulates fatty acid synthesis by stabilizing wrinkled1[open]. Plant Cell **30**.

Zhai, Z., Liu, H., and Shanklin, J. (2021). Ectopic expression of oleosin 1 and inactivation of gbss1 have a synergistic effect on oil accumulation in plant leaves. Plants **10**.

Zhai, Z., Liu, H., and Shanklin, J. (2017a). Phosphorylation of WRINKLED1 by KIN10 results in its proteasomal degradation, providing a link between energy homeostasis and lipid biosynthesis. Plant Cell **29**.

Zhai, Z., Liu, H., Xu, C., and Shanklin, J. (2017b). Sugar potentiation of fatty acid and triacylglycerol accumulation. Plant Physiol. **175**.

Zhang, H., Liu, Y., Fields, L., Shi, X., Huang, P., Lu, H., Schneider, A.J., Tang, X., Puglielli, L., Welham, N. V., and Li, L. (2023). Single-cell lipidomics enabled by dual-polarity ionization and ion mobility-mass spectrometry imaging. Nat. Commun. **14**: 5185.

Zhang, J., Chen, Y., Fu, L., Guo, E., Wang, B., Dai, L., and Si, T. (2021). Accelerating strain engineering in biofuel research via build and test automation of synthetic biology. Curr. Opin. Biotechnol. **67**.

Zhang, S., Skerker, J.M., Rutter, C.D., Maurer, M.J., Arkin, A.P., and Rao, C. V. (2016). Engineering Rhodosporidium toruloides for increased lipid production. Biotechnol. Bioeng. **113**.

Zhang, X., Pan, S.R., Hu, H.M., Wu, G.F., Feng, M., Zhang, W., and Luo, X. (2008). Poly(ethylene glycol)-block-polyethylenimine copolymers as carriers for gene delivery: Effects of PEG molecular weight and PEGylation degree. J. Biomed. Mater. Res. - Part A **84**.

1165

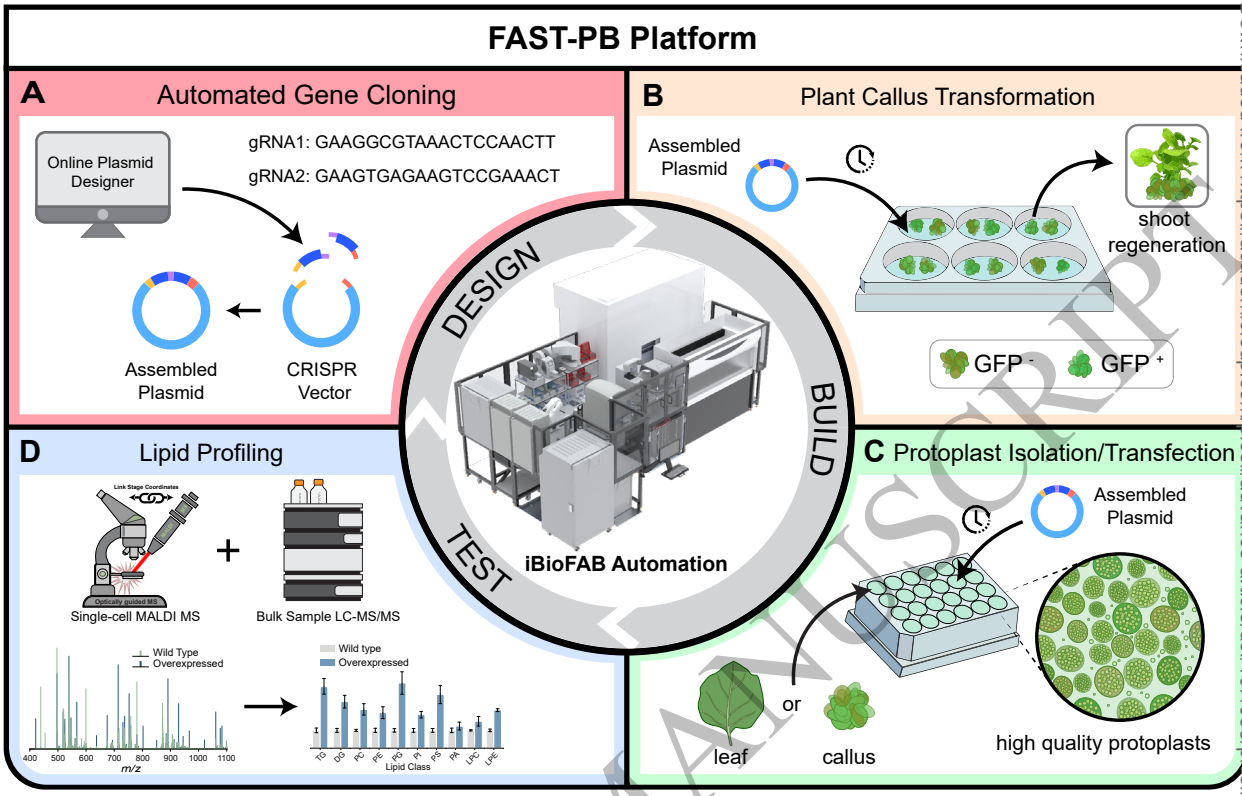

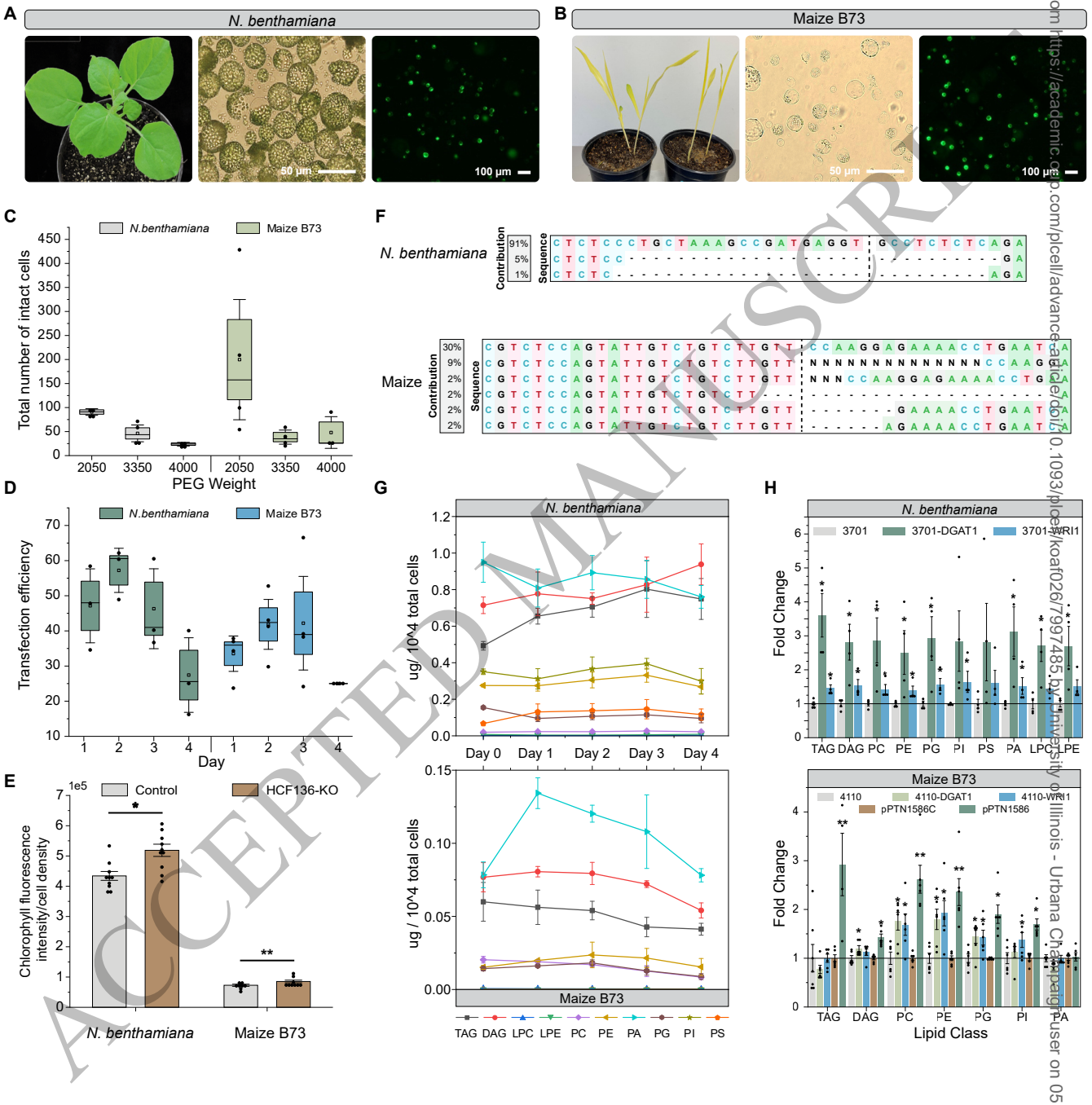

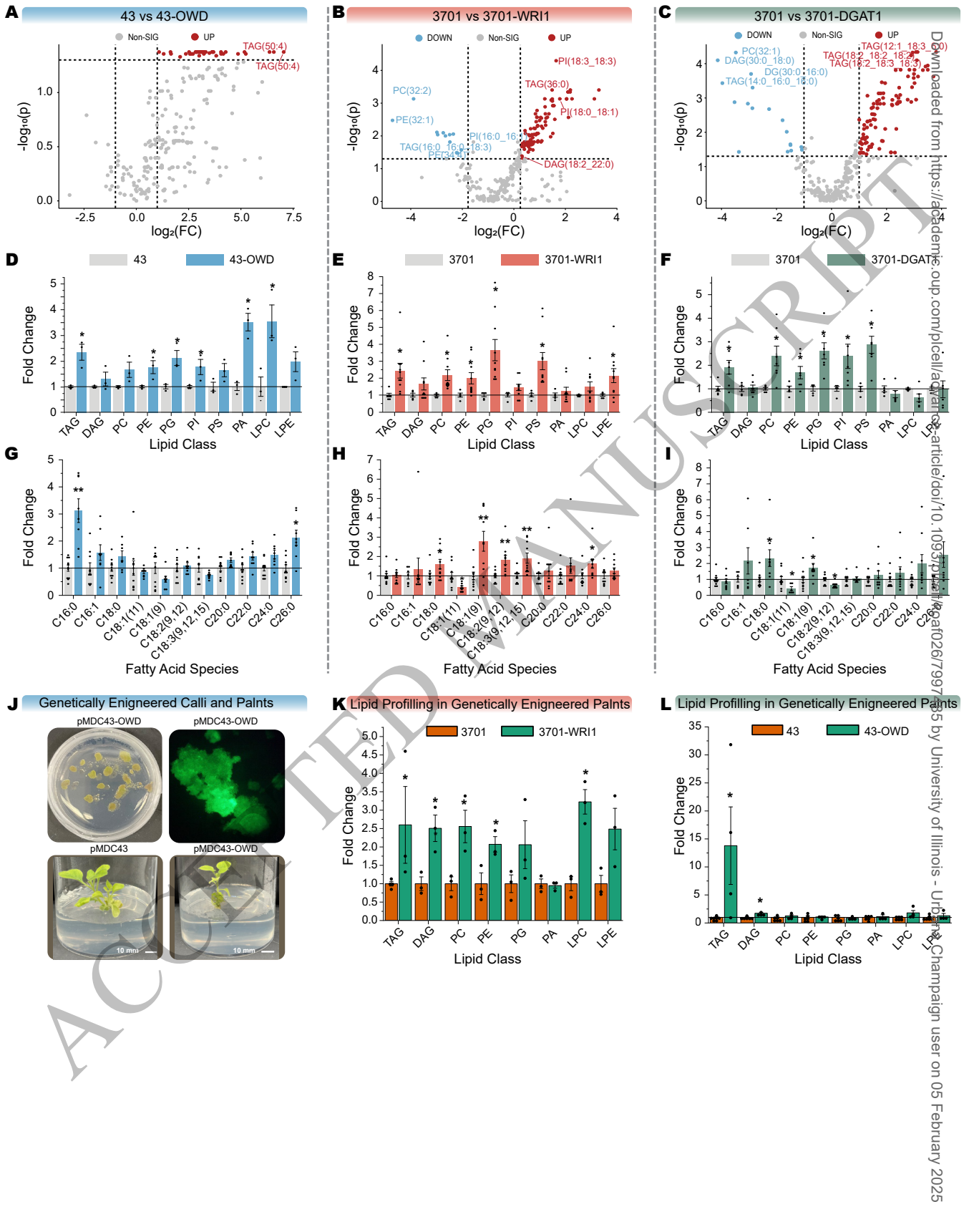

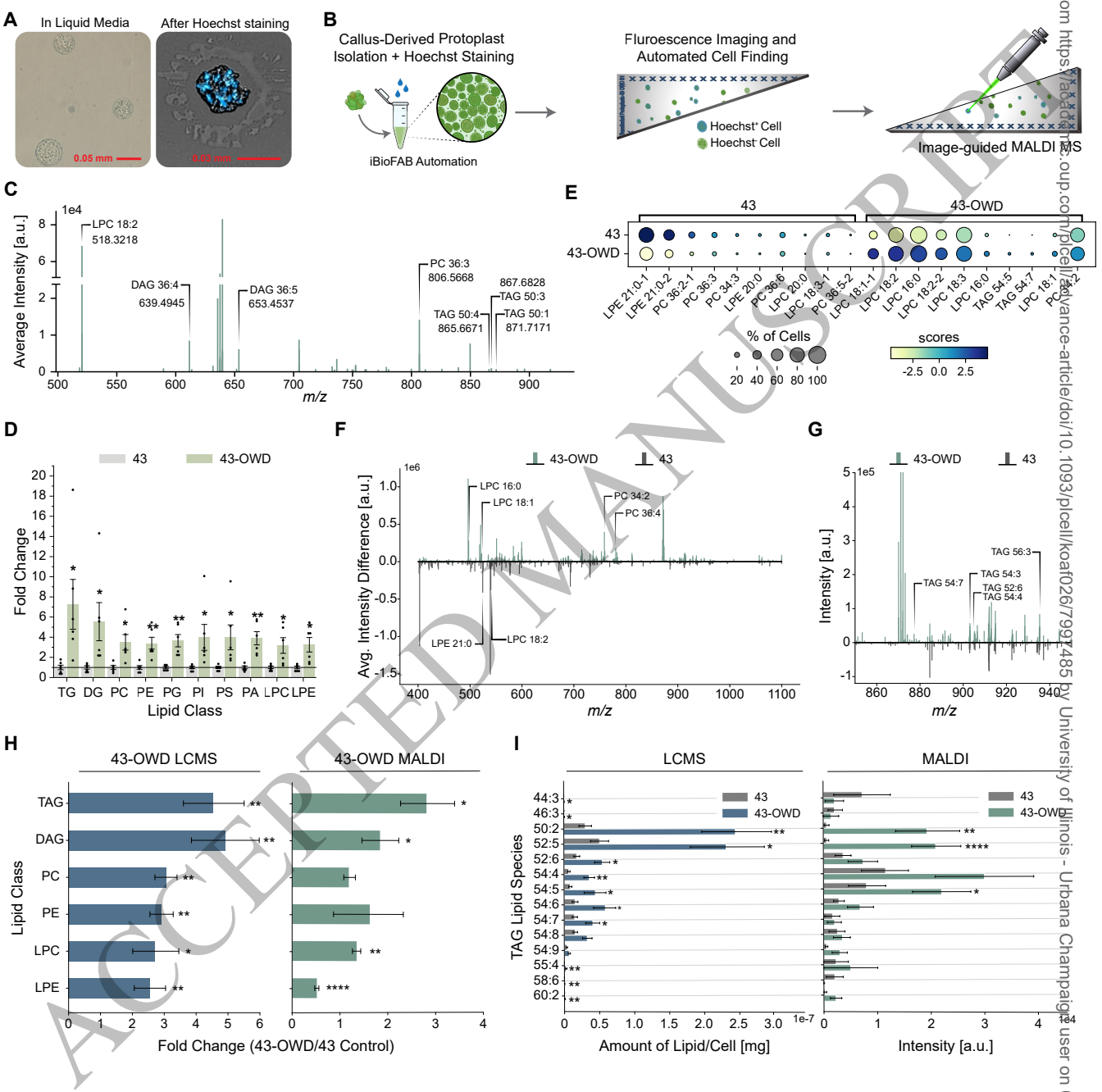

Parsed Citations

Ali, A., Abouleila, Y., Shimizu, Y., Hiyama, E., Emara, S., Mashaghi, A., and Hankemeier, T. (2019). Single-cell metabolomics by mass spectrometry: Advances, challenges, and future applications. TrAC - Trends Anal. Chem. 120.
Google Scholar: Author Only Title Only Author and Title

An, G. (1985). High Efficiency Transformation of Cultured Tobacco Cells. Plant Physiol. 79.
Google Scholar: Author Only Title Only Author and Title

Bourceau, P., Geier, B., Suerdieck, V., Bien, T., Soltwisch, J., Dreisewerd, K., and Liebeke, M. (2023). Visualization of metabolites and microbes at high spatial resolution using MALDI mass spectrometry imaging and in situ fluorescence labeling. Nat. Protoc.
Google Scholar: Author Only Title Only Author and Title

Cai, Y., Goodman, J.M., Pyc, M., Mullen, R.T., Dyer, J.M., and Chapmana, K.D. (2015). Arabidopsis SEIPIN proteins modulate triacylglycerol accumulation and influence lipid droplet proliferation. Plant Cell 27.
Google Scholar: Author Only Title Only Author and Title

Castro, D.C., Chan-Andersen, P., Romanova, E. V., and Sweedler, J. V. (2023). Probe-based mass spectrometry approaches for single-cell and single-organelle measurements. Mass Spectrom. Rev.
Google Scholar: Author Only Title Only Author and Title

Castro, D.C., Xie, Y.R., Rubakhin, S.S., Romanova, E. V., and Sweedler, J. V. (2021). Image-guided MALDI mass spectrometry for high-throughput single-organelle characterization. Nat. Methods 18.
Google Scholar: Author Only Title Only Author and Title

Čermák, T., Curtin, S.J., Gil-Humanes, J., Čegan, R., Kono, T.J.Y., Konečná, E., Belanto, J.J., Starker, C.G., Mathre, J.W., Greenstein, R.L., and Voytas, D.F. (2017). A multipurpose toolkit to enable advanced genome engineering in plants. Plant Cell 29.
Google Scholar: Author Only Title Only Author and Title

Chao, R., Mishra, S., Si, T., and Zhao, H. (2017). Engineering biological systems using automated biofoundries. Metab. Eng. 42.
Google Scholar: Author Only Title Only Author and Title

Chapman, K.D. and Ohlrogge, J.B. (2012). Compartmentation of triacylglycerol accumulation in plants. J. Biol. Chem. 287.
Google Scholar: Author Only Title Only Author and Title

Clemente, T. (2006). Nicotiana (Nicotiana tobaccum, Nicotiana benthamiana). In Agrobacterium Protocols.
Google Scholar: Author Only Title Only Author and Title

Cole, B. et al. (2021). Plant single-cell solutions for energy and the environment. Commun. Biol. 4.
Google Scholar: Author Only Title Only Author and Title

Comi, T.J., Neumann, E.K., Do, T.D., and Sweedler, J. V. (2017). microMS: A Python Platform for Image-Guided Mass Spectrometry Profiling. J. Am. Soc. Mass Spectrom. 28.
Google Scholar: Author Only Title Only Author and Title

Conant, D., Hsiau, T., Rossi, N., Oki, J., Maures, T., Waite, K., Yang, J., Joshi, S., Kelso, R., Holden, K., Enzmann, B.L., and Stoner, R. (2022). Inference of CRISPR Edits from Sanger Trace Data. Cris. J. 5.
Google Scholar: Author Only Title Only Author and Title

Cui, Y., Gao, J., He, Y., and Jiang, L. (2020). Plant extracellular vesicles. Protoplasma 257.
Google Scholar: Author Only Title Only Author and Title

Demirer, G.S., Zhang, H., Matos, J.L., Goh, N.S., Cunningham, F.J., Sung, Y., Chang, R., Aditham, A.J., Chio, L., Cho, M.J., Staskawicz, B., and Landry, M.P. (2019). High aspect ratio nanomaterials enable delivery of functional genetic material without DNA integration in mature plants. Nat. Nanotechnol. 14.
Google Scholar: Author Only Title Only Author and Title

Dong, J., Zielinski, R.E., and Hudson, M.E. (2020). t-SNAREs Bind the Rhg1 α-SNAP and Mediate Soybean Cyst Nematode Resistance. Plant J. cell Mol. Biol.
Google Scholar: Author Only Title Only Author and Title

Eberwine, J. et al. (2023). Subcellular omics: a new frontier pushing the limits of resolution, complexity and throughput. Nat. Methods 20.
Google Scholar: Author Only Title Only Author and Title

Enghiad, B., Xue, P., Singh, N., Boob, A.G., Shi, C., Petrov, V.A., Liu, R., Peri, S.S., Lane, S.T., Gaither, E.D., and Zhao, H. (2022). PlasmidMaker is a versatile, automated, and high throughput end-to-end platform for plasmid construction. Nat. Commun. 13.
Google Scholar: Author Only Title Only Author and Title

Guo, S., Zhang, C., and Le, A. (2021). The limitless applications of single-cell metabolomics. Curr. Opin. Biotechnol. 71.

Google Scholar: Author Only Title Only Author and Title

Hajdukiewicz, P., Svab, Z., and Maliga, P. (1994). The small, versatile pPZP family of Agrobacterium binary vectors for plant transformation. Plant Mol. Biol. 25.
Google Scholar: Author Only Title Only Author and Title

Hillson, N. et al. (2019). Building a global alliance of biofoundries. Nat. Commun. 10.
Google Scholar: Author Only Title Only Author and Title

Hsiau, T., Maures, T., Waite, K., Yang, J., Kelso, R., Holden, K., and Stoner, R. (2018). Inference of CRISPR Edits from Sanger Trace Data. bioRxiv: 251082.
Google Scholar: Author Only Title Only Author and Title

Huang, Y., Shang, M., Liu, T., and Wang, K. (2022). High-throughput methods for genome editing: The more the better. Plant Physiol. 188.
Google Scholar: Author Only Title Only Author and Title

Ikeuchi, M., Sugimoto, K., and Iwase, A. (2013). Plant callus: Mechanisms of induction and repression. Plant Cell 25.
Google Scholar: Author Only Title Only Author and Title

Jacobs, T.B., LaFayette, P.R., Schmitz, R.J., and Parrott, W.A. (2015). Targeted genome modifications in soybean with CRISPR/Cas9. BMC Biotechnol. 15.
Google Scholar: Author Only Title Only Author and Title

Karlson, C.K.S., Mohd-noor, S.N., Nolte, N., and Tan, B.C. (2021). Crispr/dcas9-based systems: Mechanisms and applications in plant sciences. Plants 10.
Google Scholar: Author Only Title Only Author and Title

Lawson, D.A. et al. (2015). Single-cell analysis reveals a stem-cell program in human metastatic breast cancer cells. Nature 526.
Google Scholar: Author Only Title Only Author and Title

Lei, Y., Lu, L., Liu, H.Y., Li, S., Xing, F., and Chen, L.L. (2014). CRISPR-P: A web tool for synthetic single-guide RNA design of CRISPR-system in plants. Mol. Plant 7: 1494–1496.
Google Scholar: Author Only Title Only Author and Title

Lenaghan, S.C. and Neal Stewart, C. (2019). An automated protoplast transformation system. In Methods in Molecular Biology.
Google Scholar: Author Only Title Only Author and Title

Liu, D., Shi, L., Han, C., Yu, J., Li, D., and Zhang, Y. (2012). Validation of Reference Genes for Gene Expression Studies in Virus-Infected Nicotiana benthamiana Using Quantitative Real-Time PCR. PLoS One 7.
Google Scholar: Author Only Title Only Author and Title

Livak, K.J. and Schmittgen, T.D. (2001). Analysis of relative gene expression data using real-time quantitative PCR and the 2-ΔΔCT method. Methods 25: 402–408.
Google Scholar: Author Only Title Only Author and Title

Lu, Y., Pang, Z., and Xia, J. (2023). Comprehensive investigation of pathway enrichment methods for functional interpretation of LC-MS global metabolomics data. Brief. Bioinform. 24.
Google Scholar: Author Only Title Only Author and Title

Maitra, S., Viswanathan, M.B., Park, K., Kannan, B., Alfanar, S.C., McCoy, S.M., Cahoon, E.B., Altpeter, F., Leakey, A.D.B., and Singh, V. (2022). Bioprocessing, Recovery, and Mass Balance of Vegetative Lipids from Metabolically Engineered "oilcane" Demonstrates Its Potential as an Alternative Feedstock for Drop-In Fuel Production. ACS Sustain. Chem. Eng. 10.
Google Scholar: Author Only Title Only Author and Title

Mamode Cassim, A. and Mongrand, S. (2019). Lipids light up in plant membranes. Nat. Plants 5.
Google Scholar: Author Only Title Only Author and Title

Manoli, A., Sturaro, A., Trevisan, S., Quaggiotti, S., and Nonis, A. (2012). Evaluation of candidate reference genes for qPCR in maize. J. Plant Physiol. 169.
Google Scholar: Author Only Title Only Author and Title

Martín-Saiz, L. et al. (2023). Using the Synergy between HPLC-MS and MALDI-MS Imaging to Explore the Lipidomics of Clear Cell Renal Cell Carcinoma. Anal. Chem. 95.
Google Scholar: Author Only Title Only Author and Title

Meurer, J., Plücken, H., Kowallik, K. V., and Westhoff, P. (1998). A nuclear-encoded protein of prokaryotic origin is essential for the stability of photosystem II in Arabidopsis thaliana. EMBO J. 17.
Google Scholar: Author Only Title Only Author and Title

Mumm, R.H. (2013). A look at product development with genetically modified crops: Examples from maize. J. Agric. Food Chem.

61.
Google Scholar: Author Only Title Only Author and Title

Murashige, T. and Skoog, F. (1962). A Revised Medium for Rapid Growth and Bio Assays with Tobacco Tissue Cultures. Physiol. Plant. 15.
Google Scholar: Author Only Title Only Author and Title

Napier, J.A., Haslam, R.P., Beaudoin, F., and Cahoon, E.B. (2014). Understanding and manipulating plant lipid composition: Metabolic engineering leads the way. Curr. Opin. Plant Biol. 19.
Google Scholar: Author Only Title Only Author and Title

Neumann, E.K., Do, T.D., Comi, T.J., and Sweedler, J. V. (2019). Exploring the Fundamental Structures of Life: Non-Targeted, Chemical Analysis of Single Cells and Subcellular Structures. Angew. Chemie - Int. Ed. 58.
Google Scholar: Author Only Title Only Author and Title

Norouzi, O., Hesami, M., Pepe, M., Dutta, A., and Jones, A.M.P. (2022). In vitro plant tissue culture as the fifth generation of bioenergy. Sci. Rep. 12.
Google Scholar: Author Only Title Only Author and Title

Pandian, K., Matsui, M., Hankemeier, T., Ali, A., and Okubo-Kurihara, E. (2023). Advances in single-cell metabolomics to unravel cellular heterogeneity in plant biology. Plant Physiol.
Google Scholar: Author Only Title Only Author and Title

Raczyk, M. and Rudzińska, M. (2015). Analysis of plant lipids. Plant Lipids Sci. Technol. Nutr. Value Benefits to Hum. Heal. 661.
Google Scholar: Author Only Title Only Author and Title

Rigoulot, S.B. et al. (2023). Automated, High-Throughput Protoplast Transfection for Gene Editing and Transgene Expression Studies. In Plant Genome Engineering. Methods in Molecular Biology, S.B. Rigoulot, ed (Humana, New York, NY.), pp. 129–149.
Google Scholar: Author Only Title Only Author and Title

Roy, A.L., Conroy, R., Smith, J., Yao, Y., Beckel-Mitchener, A.C., Anderson, J.M., and Wilder, E.L. (2018). Accelerating a paradigm shift: The common fund single cell analysis program. Sci. Adv. 4.
Google Scholar: Author Only Title Only Author and Title

Sarrion-Perdigones, A., Vazquez-Vilar, M., Palací, J., Castelijns, B., Forment, J., Ziarsolo, P., Blanca, J., Granell, A., and Orzaez, D. (2013). Goldenbraid 2.0: A comprehensive DNA assembly framework for plant synthetic biology. Plant Physiol. 162.
Google Scholar: Author Only Title Only Author and Title

Seydel, C. (2021). Single-cell metabolomics hits its stride. Nat. Methods 18.
Google Scholar: Author Only Title Only Author and Title

Si, T., Chao, R., Min, Y., Wu, Y., Ren, W., and Zhao, H. (2017). Automated multiplex genome-scale engineering in yeast. Nat. Commun.
Google Scholar: Author Only Title Only Author and Title

Si, T., Xiao, H., and Zhao, H. (2015). Rapid prototyping of microbial cell factories via genome-scale engineering. Biotechnol. Adv. 33.
Google Scholar: Author Only Title Only Author and Title

Squire, H.J., Tomatz, S., Voke, E., González-Grandío, E., and Landry, M. (2023). The emerging role of nanotechnology in plant genetic engineering. Nat. Rev. Bioeng. 1.
Google Scholar: Author Only Title Only Author and Title

Taylor, M.J., Lukowski, J.K., and Anderton, C.R. (2021). Spatially Resolved Mass Spectrometry at the Single Cell: Recent Innovations in Proteomics and Metabolomics. J. Am. Soc. Mass Spectrom. 32.
Google Scholar: Author Only Title Only Author and Title

TSAI, C.H., WEN, M.C., and KINSELLA, J.E. (1982). Cocobean Tissue Culture: Lipid Composition and Fatty Acid Metabolism. J. Food Sci. 47.
Google Scholar: Author Only Title Only Author and Title

Tsugawa, H. et al. (2020). A lipidome atlas in MS-DIAL 4. Nat. Biotechnol. 38.
Google Scholar: Author Only Title Only Author and Title

Urzì, O., Raimondo, S., and Alessandro, R. (2021). Extracellular vesicles from plants: Current knowledge and open questions. Int. J. Mol. Sci. 22.
Google Scholar: Author Only Title Only Author and Title

Vanhercke, T. et al. (2014). Metabolic engineering of biomass for high energy density: Oilseed-like triacylglycerol yields from plant leaves. Plant Biotechnol. J. 12.
Google Scholar: Author Only Title Only Author and Title

Vanhercke, T., Dyer, J.M., Mullen, R.T., Kilaru, A., Rahman, M.M., Petrie, J.R., Green, A.G., Yurchenko, O., and Singh, S.P. (2019). Metabolic engineering for enhanced oil in biomass. Prog. Lipid Res. 74.
Google Scholar: Author Only Title Only Author and Title

Volk, M.J., Tran, V.G., Tan, S.I., Mishra, S., Fatma, Z., Boob, A., Li, H., Xue, P., Martin, T.A., and Zhao, H. (2023). Metabolic Engineering: Methodologies and Applications. Chem. Rev. 123.
Google Scholar: Author Only Title Only Author and Title

Xue, P., Si, T., Mishra, S., Zhang, L., Choe, K., Sweedler, J. V., and Zhao, H. (2020). A mass spectrometry-based high-throughput screening method for engineering fatty acid synthases with improved production of medium-chain fatty acids. Biotechnol. Bioeng. 117.
Google Scholar: Author Only Title Only Author and Title

Yin, K., Gao, C., and Qiu, J.L. (2017). Progress and prospects in plant genome editing. Nat. Plants 3.
Google Scholar: Author Only Title Only Author and Title

Zhai, Z., Keereetaweep, J., Liu, H., Feil, R., Lunn, J.E., and Shanklin, J. (2018). Trehalose 6-phosphate positively regulates fatty acid synthesis by stabilizing wrinkled1[open]. Plant Cell 30.
Google Scholar: Author Only Title Only Author and Title

Zhai, Z., Liu, H., and Shanklin, J. (2021). Ectopic expression of oleosin 1 and inactivation of gbss1 have a synergistic effect on oil accumulation in plant leaves. Plants 10.
Google Scholar: Author Only Title Only Author and Title

Zhai, Z., Liu, H., and Shanklin, J. (2017a). Phosphorylation of WRINKLED1 by KIN10 results in its proteasomal degradation, providing a link between energy homeostasis and lipid biosynthesis. Plant Cell 29.
Google Scholar: Author Only Title Only Author and Title

Zhai, Z., Liu, H., Xu, C., and Shanklin, J. (2017b). Sugar potentiation of fatty acid and triacylglycerol accumulation. Plant Physiol. 175.
Google Scholar: Author Only Title Only Author and Title

Zhang, H., Liu, Y., Fields, L., Shi, X., Huang, P., Lu, H., Schneider, A.J., Tang, X., Puglielli, L., Welham, N. V., and Li, L. (2023). Single-cell lipidomics enabled by dual-polarity ionization and ion mobility-mass spectrometry imaging. Nat. Commun. 14: 5185.
Google Scholar: Author Only Title Only Author and Title

Zhang, J., Chen, Y., Fu, L., Guo, E., Wang, B., Dai, L., and Si, T. (2021). Accelerating strain engineering in biofuel research via build and test automation of synthetic biology. Curr. Opin. Biotechnol. 67.
Google Scholar: Author Only Title Only Author and Title

Zhang, S., Skerker, J.M., Rutter, C.D., Maurer, M.J., Arkin, A.P., and Rao, C. V. (2016). Engineering Rhodosporidium toruloides for increased lipid production. Biotechnol. Bioeng. 113.
Google Scholar: Author Only Title Only Author and Title

Zhang, X., Pan, S.R., Hu, H.M., Wu, G.F., Feng, M., Zhang, W., and Luo, X. (2008). Poly(ethylene glycol)-block-polyethylenimine copolymers as carriers for gene delivery: Effects of PEG molecular weight and PEGylation degree. J. Biomed. Mater. Res. - Part A 84.
Google Scholar: Author Only Title Only Author and Title